11606 *Inorg. Chem.* **2010**, *49*, 11606–11618
DOI: 10.1021/ic102000s

Inorganic Chemistry
Article

High-Nuclearity Pt−Tl−Fe Complexes: Structural, Electrochemistry, and Spectroelectrochemistry Studies

Álvaro Díez, Julio Fernández, Elena Lalinde,* M. Teresa Moreno,* and Sergio Sánchez

Departamento de Química—Grupo de Síntesis Química de La Rioja, UA—CSIC, Universidad de La Rioja, 26006, Logroño, Spain

Received September 30, 2010

A series of heteropolynuclear Pt−Tl−Fe complexes have been synthesized and structurally characterized. The final structures strongly depend on the geometry of the precursor and the Pt/Tl ratio used. Thus, the anionic *heteroleptic cis*-configured $[cis\text{-}Pt(C_6F_5)_2(C{\equiv}CFc)_2]^{2-}$ and $[Pt(bzq)(C{\equiv}CFc)_2]^-$ (Fc = ferrocenyl) complexes react with Tl^+ to form discrete octanuclear $(PPh_3Me)_2[\{trans,cis,cis\text{-}PtTl(C_6F_5)_2(C{\equiv}CFc)_2\}_2]$ (**1**), $[PtTl(bzq)(C{\equiv}CFc)_2]_2$ (**5**; bzq = benzoquinolate), and decanuclear $[trans,cis,cis\text{-}PtTl_2(C_6F_5)_2(C{\equiv}CFc)_2]_2$ (**3**) derivatives, stabilized by both $Pt^{II}\cdots Tl^{I}$ and $Tl^{I}\cdots\eta^2$(alkynyl) bonds. By contrast, $Q_2[trans\text{-}Pt(C_6F_5)_2(C{\equiv}CFc)_2]$ (Q = NBu_4) reacts with Tl^+ to give the one-dimensional (1-D) anionic $[(NBu_4)\{trans,trans,trans\text{-}PtTl(C_6F_5)_2(C{\equiv}CFc)_2\}]_n$ (**2**) and neutral $[trans,trans,trans\text{-}PtTl_2(C_6F_5)_2(C{\equiv}CFc)_2]_n$ (**4**) polymeric chains based on $[PtFc_2]^{2-}$ platinate fragments and Tl^+ (**2**) or $[Tl\cdots Tl]^{2+}$ (**4**) units, respectively, connected by $Pt^{II}\cdots Tl^{I}$ and secondary weak $\kappa\text{-}\eta^1$ (**2**) or η^2 (**4**) alkynyl$\cdots Tl^{I}$ bonding. The formation of **1**−**4** is reversible, and thus treatment of neutral **3** and **4** with PPh_3MeBr causes the precipitation of TlBr, returning toward the formation of the anionic **1** and **2′** (Q = PPh_3Me). Two slightly different pseudopolymorphs were found for **2′**, depending on the crystallization solvent. Finally, the reaction of the *homoleptic* $[Pt(C{\equiv}CFc)_4]^{2-}$ with 2 equiv of Tl^+ affords the tetradecanuclear sandwich type complex $[Pt_2Tl_4(C{\equiv}CFc)_8]$ (**6**). Electrochemical, spectroelectrochemical, and theoretical studies have been carried out to elucidate the effect produced by the interaction of the Tl^+ with the Pt−C≡CFc fragments. The cyclic voltammetry (CV) and differential pulse voltammetry (DPV) of **1**−**5** reveal that, in general, neutralization of the anionic fragments increases the stability of the fully oxidized species and gives higher $E_{1/2}$ (Fc) values than those observed in their precursors, increasing with the number of Pt−Tl bonding interactions. However, the electronic communication between Fc groups is reduced or even lost upon Tl^+ coordination, as confirmed by electrochemical (CVs and DPVs voltammograms, **1**−**5**) and spectroelectrochemical (UV−vis−NIR, **2**−**4**) studies. Complexes **2** and **4** still display some electronic interaction between the Fc groups, supported by the presence of an IVCT band in their UV−vis−NIR spectra of oxidized species and additional comparative DFT calculations with the precursor $[trans\text{-}Pt(C_6F_5)_2(C{\equiv}CFc)_2]^{2-}$ and complex **3**.

Introduction

The synthesis of metal-based materials containing electroactive groups, conjugated molecules, or both has been extensively researched in recent years due to their potential application in the construction of molecular electronic devices.[1] In this area, π-conjugated complexes containing ethynylferrocene as capping moieties have been extensively investigated due to the well-known redox chemistry of the ferrocenyl group and the possibility of electronic interaction through the alkynyl (−C≡C−) fragments.[2−21] Several models are commonly employed to evaluate the capability of electronic communication

*To whom correspondence should be addressed. Fax: (+34)941-299621. E-mail: elena.lalinde@unirioja.es (E.L.); teresa.moreno@unirioja.es (M.T.M.).

(1) (a) Kaim, W.; Lahiri, G. K. *Angew. Chem., Int. Ed.* **2007**, *46*, 1778–1796. (b) Petty, M. C. *Molecular Electronics, from Principles to Practice*; Wiley Interscience: New York, 2008. (c) Schwab, P. F. H.; Smith, J. R.; Michl, J. *Chem. Rev.* **2005**, *105*, 1197–1280. (d) Lin, Y. C.; Chen, W. T.; Tai, J.; Su, D.; Huang, S. Y.; Lin, I.; Lin, J. L.; Lee, M. M.; Chiou, M. F.; Liu, Y. H.; Kwan, K. S.; Chen, Y. J.; Chen, H. Y. *Inorg. Chem.* **2009**, *48*, 1857–1870. (e) Ratner, M. *Nature* **2000**, *404*, 137–138. (f) Hipps, K. W. *Science* **2001**, *294*, 536–537. (g) Low, P. J. *Dalton Trans.* **2005**, 2821–2824. (h) Kaim, W.; Klein, A.; Glockle, M. *Acc. Chem. Res.* **2000**, *33*, 755–763.

(2) (a) Debroy, P.; Roy, S. *Coord. Chem. Rev.* **2007**, *251*, 203–221. (b) Sakamoto, R.; Kume, S.; Nishihara, H. *Chem.—Eur. J.* **2008**, *14*, 6978–6986. (c) Muratsugu, S.; Kume, S.; Nishihara, H. *J. Am. Chem. Soc.* **2008**, *130*, 7204–7205. (d) Engtrakul, C.; Sita, L. R. *Organometallics* **2008**, *27*, 927–937. (e) Wong, W. Y.; Lu, G. L.; Choi, K. H.; Guo, Y. H. *J. Organomet. Chem.* **2005**, *690*, 177–186. (f) Zhu, Y.; Wolf, M. O. *J. Am. Chem. Soc.* **2000**, *122*, 10121–10125. (g) Xu, G. L.; Xi, B.; Updegraff, J. B.; Protasiewicz, J. D.; Ren, T. *Organometallics* **2006**, *25*, 5213–5215.

(3) (a) Osella, D.; Gobetto, R.; Nervi, C.; Ravera, M.; D'Amato, R.; Russo, M. V. *Inorg. Chem. Commun.* **1998**, *1*, 239–245. (b) Díez, A.; Lalinde, E.; Moreno, M. T.; Sánchez, S. *Dalton Trans.* **2009**, 3434–3446.

(4) Díez, A.; Fernández, J.; Lalinde, E.; Moreno, M. T.; Sánchez, S. *Dalton Trans.* **2008**, 4926–4936.

(5) Jakob, A.; Ecorchard, P.; Linseis, M.; Winter, R. F.; Lang, H. *J. Organomet. Chem.* **2009**, *694*, 655–666.

(6) (a) Lebreton, C.; Touchard, D.; Pichon, L. L.; Daridor, A.; Toupet, L.; Dixneuf, P. H. *Inorg. Chim. Acta* **1998**, *272*, 188–196. (b) Colbert, M. C. B.; Lewis, J.; Long, N. J.; Raithby, P. R.; White, A. J. P.; Williams, D. J. *Dalton Trans.* **1997**, 99–104. (c) Zhu, Y.; Clot, O.; Wolf, M. O.; Yap, G. P. A. *J. Am. Chem. Soc.* **1998**, *120*, 1812–1821. (d) Jones, N. D.; Wolf, M. O.; Giaquinta, D. M. *Organometallics* **1997**, *16*, 1352–1354.

Published on Web 11/17/2010

between ferrocenyl groups (Fc) in ethynylferrocene derivatives, varying the nature of the spacers: (a) a π-conjugated organic spacer (Fc−C≡C−spacer−C≡C−Fc),[2] (b) a single metal ion (Fc−C≡C−M−C≡C−Fc) (M = Pt,[3−5] Ru,[6] Mn[7]), (c) an organometallic fragment in a conjugated organic chain (Fc−C≡C−spacer−M−spacer−C≡C−Fc),[8] (d) single M−M bonds, usually supported by bridging ligands (Fc−C≡C−M−M−C≡C−Fc), (M−M = Pt−Pt, Ru−Ru)[9−11] or dimetal oligomeric species (Fc−(C≡C)$_n$−M$_2$−(C≡C)$_n$−Fc),[11,12] and (e) transition metal clusters (including Cu_3,[13] Co_3,[14] Ru_3,[15] Os_3,[16] Mo_6,[17] Pt_6,[18] Ag_8/M_6 (M = Cu, Ag, Au),[19] Au_3Cu_2,[20] and Ag_6-Cu_6[21]). These studies have demonstrated that the electronic nature of the connectors, including metal centers and their ancillary ligands, plays a crucial role in the electronic coupling and, hence, electron delocalization of these species. Within this field, our group has recently investigated a series of neutral and anionic platinum(II) complexes containing two (*cis*/*trans*) or four ferrocenylethynyl groups.[4] The study of their electrochemical properties revealed the existence of higher electronic communication between the Fc moieties in the anionic complexes than in the neutral ones, but their oxidized species were found to have low stability.

On the other hand, the metal···π(alkynyl) bonding has been amply exploited in building novel molecular architectures, which may exhibit a variety of interesting properties.[22] In this respect, we and others have demonstrated that anionic alkynyl platinates are useful as building blocks to synthesize heteropolynuclear Pt−M (M = d^{10}, s^2) systems,[23−27] stabilized via $\pi(\eta^2)$-alkynyl bonds and/or Pt···M bonding interactions, with rich photoluminescent properties. It has been shown that depending on the nature of the platinate fragment and the electronic requirements of the heterometal, this latter shows a greater or lesser preference to be bonded to the alkynyl units or to the basic Pt^{II} center.

Within this framework, it is surprising that ferrocenylethynyl platinum fragments have been only scarcely utilized in the construction of heteropolymetallic arrays,[9,28] especially for those based on $\pi(\eta^2)$ bonding interactions.[29] As part of our ongoing research in heteropolynuclear alkynyl platinum complexes and our recent interest in ferrocenylethynyl platinum complexes,[4] a program was launched to investigate the reactivity of several ferrocenylethynyl platinates toward acidic metal ions. In this paper, we report the synthesis and crystallographic and NMR characterization of new polymetallic Pt−Tl−Fe systems, together with the study of their electrochemical and spectroelectrochemical behavior and DFT calculations for complexes **2**−**4**.

Experimental Section

All reactions were carried out under an Ar atmosphere using Schlenk tube techniques. Solvents were obtained from a solvent purification system (M-BRAUN MB SPS-800). IR spectra were recorded on a FT-IR Nicolet Nexus spectrometer as Nujol mulls between polyethylene sheets, and NMR spectra were recorded on either a Bruker ARX 300 or a Bruker Avance 400 spectrometer. Chemical shifts are reported in parts per million relative to external standards ($SiMe_4$, $CFCl_3$, and 85% H_3PO_4) and coupling constants in hertz. Elemental analyses were carried out on a Perkin-Elmer 2400 CHNS/O microanalyzer and MALDI-TOF spectra on a Microflex MALDI-TOF Bruker spectrometer, operating in the linear and reflector modes using dithranol as a matrix. Conductivities were measured in acetone solutions at various concentrations using a Crison GLP31 conductimeter. Cyclic voltammetry and pulse differentials were carried out in 0.1 M NBu_4PF_6 solutions as a supporting electrolyte, using a three-electrode configuration (Pt disk as a working electrode, Pt-wire counterelectrode, Ag/AgCl reference electrode) on a Voltalab PST 050. The ferrocene/ferrocenium couple served as an internal reference (+0.46 V vs Ag/AgCl). UV−visible−near-infrared spectra were recorded

(7) Belen'kaya, A. G.; Dolgushin, F. M.; Peterleitner, M. G.; Petrovskii, P. V.; Krivykh, V. V. *Russ. Chem. Bull.* **2002**, *51*, 170–174.
(8) (a) Wong, W. Y.; Lu, G. L.; Ng, K. F.; Choi, K. H.; Lin, Z. *J. Chem. Soc., Dalton Trans.* **2001**, 3250–3260. (b) Lavastre, O.; Plass, J.; Bachmann, P.; Salaheddine, A.; Moinet, C.; Dixneuf, P. H. *Organometallics* **1997**, *16*, 184–189.
(9) Yip, J. H. K.; Wu, J.; Wong, K. Y.; Ho, K. P.; Pun, C. S. N.; Vittal, J. J. *Organometallics* **2002**, *21*, 5292–5300.
(10) Xu, G. L.; DeRosa, M. C.; Crutchley, R. J.; Ren, T. *J. Am. Chem. Soc.* **2004**, *126*, 3728–3729.
(11) Xu, G. L.; Crutchley, R. J.; DeRosa, M. C.; Pan, Q. J.; Zhang, H. X.; Wang, X. P.; Ren, T. *J. Am. Chem. Soc.* **2005**, *127*, 13354–13363.
(12) (a) Ren, T. *Organometallics* **2005**, *24*, 4854–4870. (b) Xi, B.; Xu, G. L.; Fanwick, P. E.; Ren, T. *Organometallics* **2009**, *28*, 2338–2341.
(13) Yip, J. H. K.; Wu, J.; Wong, K. Y.; Yeung, K. W.; Vittal, J. J. *Organometallics* **2002**, *21*, 1612–1621.
(14) Berry, J. F.; Cotton, F. A.; Murillo, C. A. *Organometallics* **2004**, *23*, 2503–2506.
(15) Kuo, C. K.; Chang, J. C.; Yeh, C. Y.; Lee, G. H.; Wang, C. C.; Peng, S. M. *Dalton Trans.* **2005**, 3696–3701.
(16) (a) Adams, R. D.; Qu, B. *Organometallics* **2000**, *19*, 2411–2413. (b) Adams, R. D.; Qu, B. *Organometallics* **2000**, *19*, 4090–4094.
(17) Prokopuk, N.; Shriver, D. F. *Inorg. Chem.* **1997**, *36*, 5609–5613.
(18) Albinati, A.; Fabrizi de Biani, F.; Leoni, P.; Marchetti, L.; Pasquali, M.; Rizzato, S.; Zanello, P. *Angew. Chem., Int. Ed.* **2005**, *44*, 5701–5705.
(19) Wei, Q. H.; Yin, G. Q.; Zhang, L. Y.; Chen, Z. N. *Organometallics* **2006**, *25*, 4941–4944.
(20) Koshevoy, I. O.; Smirnova, E. S.; Doménech, A.; Karttunen, A. J.; Haukka, M.; Tunik, S. P.; Pakkanen, T. A. *Dalton Trans.* **2009**, 8392–8398.
(21) Wei, Q. H.; Zhang, L. Y.; Shi, L. X.; Chen, Z. N. *Inorg. Chem. Commun.* **2004**, *7*, 286–288.
(22) (a) Berenguer, J. R.; Lalinde, E.; Moreno, M. T. *Coord. Chem. Rev.* **2010**, *254*, 832–875. (b) Belluco, U.; Bertani, R.; Michelin, P. A.; Mozzon, M. *J. Organomet. Chem.* **2000**, *600*, 37–55. (c) Lang, H.; George, D. S. A.; Rheinwald, G. *Coord. Chem. Rev.* **2000**, *206*−*207*, 101–197. (d) Michel, D.; Mingos, P.; Vilar, R.; Rais, D. *J. Organomet. Chem.* **2002**, *641*, 1216. (e) Long, N. J.; Williams, C. K. *Angew. Chem., Int. Ed. Engl.* **2003**, *42*, 2586–2617. (f) Bruce, M. I.; Low, P. J. *Adv. Organomet. Chem.* **2004**, *50*, 179–184. (g) Rosenthal, U. *Angew. Chem., Int. Ed. Engl.* **2003**, *42*, 1794–1798. (h) Mathur, P.; Chatterjee, S.; Avasare, V. D. *Adv. Organomet. Chem.* **2007**, *55*, 201–227. (i) Bruce, M. I.; Gaudio, M.; Melino, G.; Zaitseva, N. N.; Nicholson, B. K.; Skelton, B. W.; White, A. H. *J. Clust. Sci* **2008**, *19*, 147–170. (j) Wong, W. Y. *Coord. Chem. Rev.* **2007**, *251*, 2400–2427. (k) Yam, V. W. W.; Lo, K. K. W. *Chem. Soc. Rev.* **1999**, *28*, 323–334. (l) Yam, V. W. W.; Lo, K. K. W.; Wong, K. M. C. *J. Organomet. Chem.* **1999**, *578*, 3–30. (m) Yam, V. W. W. *J. Organomet. Chem.* **2004**, *689*, 1393–1401. (n) Wong, W. Y. *Dalton Trans.* **2007**, 4495–4510. (o) Chen, Z. N.; Zhao, N.; Fan, Y.; Ni, J. *Coord. Chem. Rev.* **2009**, *253*, 1–20.
(23) (a) Ara, I.; Berenguer, J. R.; Eguizábal, E.; Forniés, J.; Gómez, J.; Lalinde, E. *J. Organomet. Chem.* **2003**, *670*, 221–234. (b) Forniés, J.; Fuertes, S.; Martín, A.; Sicilia, V.; Lalinde, E.; Moreno, M. T. *Chem.—Eur. J.* **2006**, *12*, 8253–8266. (c) Charmant, J. P. H.; Forniés, J.; Gómez, J.; Lalinde, E.; Merino, R. I.; Moreno, M. T.; Orpen, A. G. *Organometallics* **1999**, *18*, 3353–3358. (d) Gil, B.; Forniés, J.; Gómez, J.; Lalinde, E.; Martín, A.; Moreno, M. T. *Inorg. Chem.* **2006**, *45*, 7788–7798. (e) Fernández, J.; Forniés, J.; Gil, B.; Gómez, J.; Lalinde, E.; Moreno, M. T. *Organometallics* **2006**, *25*, 2274–2283. (f) Forniés, J.; Ibáñez, S.; Martín, A.; Gil, B.; Lalinde, E.; Moreno, M. T. *Organometallics* **2004**, *23*, 3963–3975. (g) Berenguer, J. R.; Gil, B.; Fernández, J.; Forniés, J.; Lalinde, E. *Inorg. Chem.* **2009**, *48*, 5250–5262.
(24) (a) Charmant, J. P. H.; Forniés, J.; Gómez, J.; Lalinde, E.; Merino, R. I.; Moreno, M. T.; Orpen, A. G. *Organometallics* **2003**, *22*, 652–656. (b) Ara, I.; Berenguer, J. R.; Forniés, J.; Gómez, J.; Lalinde, E.; Merino, R. I. *Inorg. Chem.* **1997**, *36*, 6461–6464.
(25) Forniés, J.; Fuertes, S.; Martín, A.; Sicilia, V.; Gil, B.; Lalinde, E. *Dalton Trans.* **2009**, 2224–2234.
(26) Berenguer, J. R.; Forniés, J.; Gómez, J.; Lalinde, E.; Moreno, M. T. *Organometallics* **2001**, *20*, 4847–4851.
(27) Berenguer, J. R.; Forniés, J.; Gil, B.; Lalinde, E. *Chem.—Eur. J.* **2006**, *12*, 785–795.
(28) Packheiser, R.; Ecorchard, P.; Rüffer, T.; Lang, H. *Organometallics* **2008**, *27*, 3534–3546.
(29) Jakob, A.; Ecorchard, P.; Köhler, K.; Lang, H. *J. Organomet. Chem.* **2008**, *693*, 3479–3489.

on a Shimadzu UV-3600 spectrometer in a home-built optically transparent thin layer electrolysis (OTTLE) cell. Starting materials $(NBu_4)_2$[*trans*-$Pt(C_6F_5)_2(C{\equiv}CFc)_2$], $(PMePh_3)_2$[*cis*-$Pt(C_6F_5)_2(C{\equiv}CFc)_2$], (NBu_4)[$Pt(bzq)(C{\equiv}CFc)_2$], and $(NBu_4)_2$-[$Pt(C{\equiv}CFc)_4$] were prepared as previously described.[4]

Synthesis of $(PPh_3Me)_2$[{*trans*,*cis*,*cis*-$PtTl(C_6F_5)_2(C{\equiv}CFc)_2$}$_2$] (1). $TlPF_6$ (0.026 g, 0.073 mmol) was added to a solution of $(PPh_3Me)_2$[*cis*-$Pt(C_6F_5)_2(C{\equiv}CFc)_2$] (0.110 g, 0.073 mmol) in acetone (20 mL) at room temperature, and the mixture was stirred for 5 h. The solution was concentrated *in vacuo* (∼ 5 mL), and the resulting orange precipitate was filtered and washed with Et_2O (0.085 g, 81% yield). Complex **1** can be alternatively synthesized by the addition of $(PPh_3Me)Br$ (0.020 g, 0.074 mmol) to a solution of **3** (0.100 g, 0.074 mmol) in acetone (0.092 g, 88% yield). Anal. Calcd for $C_{55}H_{36}F_{10}Fe_2PPtTl$: C, 46.23; H, 2.54. Found: C, 46.57; H, 2.42%. MALDI-TOF (−): *m*/*z* (%) 1152 $[PtTl(C_6F_5)_2(C{\equiv}CFc)_2]^-$ (100). IR (cm^{-1}): ν(C≡C) 2113 (sh), 2089 (m); $\nu(C_6F_{5\ Xsens})$ 787 (m); 772 (m). Λ_M (5×10^{-4} M acetone solution): 197.1 $\Omega^{-1}cm^2\ mol^{-1}$. ^1H NMR (300.1 MHz; CD_3COCD_3): δ 7.97−7.79 (m, 15H, Ph), 4.29 (s, 4H, C_5H_4), 4.05 (s, 10H, Cp), 3.86 (s, 4H, C_5H_4), 3.24 (d, 3H, $^2J_{H-P} \sim 14$, Me, $PMePh_3$). ^{19}F NMR (376.5 MHz; CD_3COCD_3, 313 K): δ −108.6 (dm, $^3J_{Pt-Fo} \sim 308$, $4F_o$), −162.8 (m, $4F_m$), −163.6 (t, $2F_p$). ^{19}F NMR (298 K): δ −108.2 (br, $4F_o$), −162.7 (m, $4F_m$), −163.5 (t, $2F_p$). The *ortho* fluorine signal (and also the *meta*-F) resolves into two different signals at a low temperature (193 K): δ −106.2 (d, $J_{F-Tl} \sim 3300$, $^3J_{F-Pt} \sim 230$, 2 *endo*-F_o), −107.6 (d, $^4J_{F_o\text{-}Tl} \sim 95$, $^3J_{F_o\text{-}Pt} \sim 355$, 2 *exo*-$F_o$), −161.3 (m, $2F_m$), −161.7 (m, $2F'_m$), −167.0 (m $2F_p$) (F_o: $\Delta G^{\#}$ = 52 KJ/mol, $T_{coalescence}$ = 260 K; F_m: $\Delta G^{\#}$ = 55 KJ/mol, $T_{coalescence}$ = 240 K). $^{31}P\{^1H\}$ NMR (121.5 MHz; CD_3COCD_3): 21.8 (s, $PMePh_3$).

Synthesis of [(NBu_4)]{*trans*,*trans*,*trans*-$PtTl(C_6F_5)_2(C{\equiv}CFc)_2$}$_n$ (2). This compound was prepared as an orange solid using the method described for **1**, starting from $TlPF_6$ (0.024 g, 0.070 mmol) and $(NBu_4)_2$[*trans*-$Pt(C_6F_5)_2(C{\equiv}CFc)_2$] (0.100 g, 0.070 mmol; 0.079 g, 81% yield). Anal. Calcd for $C_{52}H_{54}F_{10}Fe_2PtNTl$: C, 44.80; H, 3.90; N, 1.00. Found: C, 44.65; H, 3.80; N 1.01%. MALDI-TOF (−): *m*/*z* (%) 1152 $[PtTl(C_6F_5)_2(C{\equiv}CFc)_2]^-$ (100). IR (cm^{-1}): ν(C≡C) 2094(m); $\nu(NBu_4)$ 880 (m); $\nu(C_6F_{5\ Xsens})$ 767 (m). Λ_M (5×10^{-4} M acetone solution): 93 $\Omega^{-1}cm^2\ mol^{-1}$. ^1H NMR (300.1 MHz; CD_3COCD_3): δ 4.00 (s, 4H, C_5H_4), 3.95 (s, 10H, Cp), 3.88 (s, 4H, C_5H_4), 3.44 (m, 8H, NCH_2-, NBu_4), 1.82 (m, 8H, $-CH_2-$, NBu_4), 1.44 (m, 8H, $-CH_2-$, NBu_4), 0.98 (t, 12H, $-CH_3$, NBu_4). ^{19}F NMR (376.5 MHz; CD_3COCD_3, 313 K): δ −114.1 (dm, $^3J_{Pt-F_o}$ 275, $4F_o$), −167.7 (m, $4F_m$), −168.5 (t, $2F_p$). ^{19}F NMR (298 K): δ −113.1 (m, $4F_o$), −166.8 (m, $4F_m$), −167.6 (t, $2F_p$). Upon cooling, the F_o signal becomes broader and finally splits at 193 K into a broad doublet centered at δ −111.5 ($J_{F_o\text{-}Tl} \sim 3215$) and a broad singlet at −110.8 ppm (F_o: $\Delta G^{\#} \sim 42$ KJ/mol; $T_{coalescence} \sim 223$ K).

Synthesis of [(PPh_3Me)]{*trans*,*trans*,*trans*-$PtTl(C_6F_5)_2(C{\equiv}CFc)_2$}$_n$ (2′). The addition of $(PPh_3Me)Br$ (0.020 g, 0.074 mmol) to a solution of **4** (0.100 g, 0.074 mmol) in acetone induces the precipitation of TlBr and the formation of **2′** as an orange solid (0.089 g, 85% yield). Anal. Calcd for $C_{55}H_{36}F_{10}Fe_2PPtTl$: C, 46.23; H, 2.54. Found: C, 46.12; H, 2.61%. MALDI-TOF (−): *m*/*z* (%) 1152 $[PtTl(C_6F_5)_2(C{\equiv}CFc)_2]^-$ (100). IR (cm^{-1}): ν(C≡C) 2094 (m); $\nu(C_6F_{5\ Xsens})$ 767 (m). Λ_M (5×10^{-4} M acetone solution): 101 $\Omega^{-1}cm^2\ mol^{-1}$. ^1H NMR (300.1 MHz; CD_3COCD_3): δ 7.97−7.75 (m, 15H, Ph), 4.01 (s, 4H, C_5H_4), 3.95 (s, 10H, Cp), 3.88 (s, 4H, C_5H_4), 3.23 (d, 3H, $^2J_{H-P} \sim 14$, Me, $PMePh_3$). ^{19}F NMR (282.4 MHz; CD_3COCD_3, 303 K): δ −113.2 (br, $4F_o$), −166.9 (m, $4F_m$), −167.6 (t, $2F_p$). ^{19}F NMR (298 K): δ −113.1 (br, $4F_o$), −166.8 (m, $4F_m$), −167.5 (t, $2F_p$). Upon cooling, the F_o signal becomes broader and finally splits at 193 K into a broad doublet centered at δ −111.9 (J_{F_o}-Tl ∼ 3200) and a broad singlet at −110.5 ppm (F_o: $\Delta G^{\#} \sim 48$ KJ/mol; $T_{coalescence} \sim 230$ K). $^{31}P\{^1H\}$ NMR (121.5 MHz; CD_3COCD_3): 21.8 (s, $PMePh_3$).

Synthesis of [*trans*,*cis*,*cis*-$PtTl_2(C_6F_5)_2(C{\equiv}CFc)_2]_2$ (3). A solution of $(PPh_3Me)_2$[*cis*-$Pt(C_6F_5)_2(C{\equiv}CFc)_2$] (0.110 g, 0.073 mmol) in acetone (20 mL) was treated with $TlPF_6$ (0.051 g, 0.146 mmol), and the mixture was stirred for 4 h. The resulting suspension was filtered, obtaining **3** as an orange solid (0.069 g, 70% yield). The same result is obtained starting from **1** (0.100 g, 0.070 mmol) and $TlPF_6$ (0.024 g, 0.070 mmol; molar Pt/Tl ratio 1:1). Anal. Calcd for $C_{36}H_{18}F_{10}Fe_2PtTl_2$: C, 31.89; H, 1.34. Found: C, 31.65; H, 1.28%. MALDI-TOF (+): *m*/*z* (%) 1152 $[PtTl(C_6F_5)_2(C{\equiv}CFc)_2]^+$ (100), 1356 $[PtTl_2(C_6F_5)_2(C{\equiv}CFc)_2]^+$ (30), 1561 $[PtTl_3(C_6F_5)_2(C{\equiv}CFc)_2]^+$ (15). Λ_M (5×10^{-4} M acetone solution): 21.3 $\Omega^{-1}cm^2\ mol^{-1}$. IR ($cm^{-1}$): ν(C≡C) 2082 (m); $\nu(C_6F_{5\ Xsens})$ 790 (m), 782 (m). ^1H NMR (300.1 MHz; CD_3COCD_3): δ 4.40 (s, 4H, C_5H_4), 4.13 (s, 10H, Cp), 4.06 (s, 4H, C_5H_4). ^{19}F NMR (376.5 MHz; CD_3COCD_3, 303 K): δ −109.5 (dm, $^3J_{Pt-F_o}$ 315, $4F_o$), −161.5 (m, $4F_m$), −161.6 (t, $2F_p$). ^{19}F NMR (298 K): δ −109.3 (m, $4F_o$), −161.5 (m, $4F_m + 2F_p$). ^{19}F NMR (193 K): δ −107.6 (dm, $J_{F-Tl(1)} = 3618$, $^3J_{F-Pt} = 220$, 2 *endo*-F_o), −107.8 (dm, br, $^4J_{F-Tl(1)} \sim 175$, $J_{F-Tl(2)} = 1970$, $^3J_{F-Pt} \sim 367$, 2 *exo*-F_o), −159.8 (m, $2F_m$), −160.1 (m, $2F'_m$), −161.0 (m, $2F_p$) (F_o: $\Delta G^{\#} = 48$ KJ/mol, $T_{coalescence}$ = 240 K).

Synthesis of [*trans*,*trans*,*trans*-$PtTl_2(C_6F_5)_2(C{\equiv}CFc)_2]_n$ (4). This complex was prepared as an orange solid using the method described for **3**, starting from $(NBu_4)_2$[*trans*-$Pt(C_6F_5)_2(C{\equiv}CFc)_2$] (0.100 g, 0.070 mmol) and 2 equiv of $TlPF_6$ (0.049 g, 0.140 mmol; 0.067 g, 70% yield), or using **2** (0.100 g, 0.072 mmol) as a precursor and 1 equiv of $TlPF_6$ (0.025 g, 0.072 mmol). Anal. Calcd. for $C_{36}H_{18}F_{10}Fe_2PtTl_2$: C, 31.89; H, 1.34. Found: C, 32.21; H, 1.33%. MALDI-TOF (+): *m*/*z* (%) 1151 $[PtTl(C_6F_5)_2(C{\equiv}CFc)_2 - H]^+$ (30), 1356 $[PtTl_2(C_6F_5)_2(C{\equiv}CFc)_2]^+$ (100), 1561 $[PtTl_3(C_6F_5)_2(C{\equiv}CFc)_2]^+$ (98). Λ_M (5×10^{-4} M acetone solution): 25.6 $\Omega^{-1}cm^2\ mol^{-1}$. IR ($cm^{-1}$): ν(C≡C) 2108 (m), 2100 (sh), 2087 (m), 2072 (s); $\nu(C_6F_{5\ Xsens})$ 772 (m). ^1H NMR (300.1 MHz; CD_3COCD_3): δ 4.11 (s, 4H, C_5H_4), 4.03 (s, 10H, Cp), 3.96 (s, 4H, C_5H_4). ^{19}F NMR (376.5 MHz; CD_3COCD_3, 298 K): δ −107.5 (dm, $^3J_{Pt-Fo}$ 272, $4F_o$), −161.0 (m, $4F_m$), −161.3 (t, $2F_p$). The *o*-F signals become broader upon cooling at 193 K, but the coalescence temperature was not achieved.

Synthesis of [$PtTl(bzq)(C{\equiv}CFc)_2]_2$ (5). To a solution of (NBu_4)-[$Pt(bzq)(C{\equiv}CFc)_2$] (0.100 g, 0.097 mmol) in acetone (20 mL) was added $TlPF_6$ (0.034 g, 0.097 mmol), and the mixture was stirred for 4 h. The orange precipitate was filtered and washed with Et_2O (0.067 g, 70% yield). Anal. Calcd. for $C_{37}H_{26}Fe_2PtNTl$: C, 44.63; H, 2.63; N, 1.41. Found: C, 44.55; H, 2.72; N 1.52%. MALDI-TOF (+): *m*/*z* (%) 995 $[PtTl(bzq)(C{\equiv}CFc)_2]^+$ (17), 1200 $[PtTl_2(bzq)(C{\equiv}CFc)_2]^+$ (100). IR (cm^{-1}): ν(C≡C) 2096 (m). Λ_M (5×10^{-4} M CH_2Cl_2 solution): 0.05 $\Omega^{-1}cm^2\ mol^{-1}$. ^1H NMR (300.1 MHz; $CDCl_3$): δ 9.75 (d, J_{H-H} 4.2, J_{Pt-H} 28.9 Hz, H^2, bzq), 8.60 (d, J_{H-H} 5.6 Hz, J_{Pt-H} 41.4, H^9, bzq), 8.29 (d, J_{H-H} 7.8, H^4, bzq), 7.84 (AB, J_{H-H} 8.7, 1H, bzq), 7.69 (m, 1H, bzq), 7.60 (AB, J_{H-H} 8.7, 1H, bzq), 7.48−7.45 (m, 2H, bzq), 4.57 (s, 2H, C_5H_4), 4.47 (s, 2H, C_5H_4), 4.25 (s, 5H, Cp), 4.19 (s, 5H, Cp), 4.17 (s, 2H, C_5H_4), 4.13 (s, 2H, C_5H_4).

Synthesis of [$Pt_2Tl_4(C{\equiv}CFc)_8$] (6). Treatment of a solution of $(NBu_4)_2$[$Pt(C{\equiv}CFc)_4$] (0.100 g, 0.066 mmol) with $TlPF_6$ (0.046 g, 0.132 mmol) in a mixture 1:1 acetone/dichloromethane (30 mL) immediately caused the precipitation of **6** as an orange solid, which was filtered and washed with acetone (0.089 g, 94% yield). Anal. Calcd. for $C_{96}H_{72}Fe_8Pt_2Tl_4$: C, 40.04; H, 2.52. Found: C, 40.21; H, 2.38%. MALDI-TOF (+): *m*/*z* (%) 1441 $[PtTl_2(C{\equiv}CFc)_4 + H]^+$ (18), 1645 $[PtTl_3(C{\equiv}CFc)_4]^+$ (100), 3085 $[Pt_2Tl_5(C{\equiv}CFc)_8]^+$ (25). IR (cm^{-1}): ν(C≡C) 2082 (s).

X-Ray Crystallography. Details of the structural analyses for **1**, **2′a**, **2′b**, **3**, **4**, **5**, and **6** are summarized in Table 1. Red crystals of **1** were obtained at −30 °C by slow diffusion of *n*-hexane into an acetone solution of the product. For complex **2′**, two different pseudopolymorphs were crystallized. Long maroon needles (**2′a**) were obtained by slow diffusion at −30 °C of Et_2O into a saturated solution of **2′**, but by the diffusion of *n*-hexane into a solution of **2′** in acetone, pale orange blocks (**2′b**) crystallized. Orange (**4** and **5**) or red (**3**) crystals were grown by diffusion of diethylether into an acetone (**3** and **4**, −30 °C) or $CHCl_3$ (**5**, room temperature)

Table 1. Crystallographic Data for **1**·2CH_3COCH_3·2C_6H_{14}, **2′a**·1.5CH_2Cl_2, **2′b**·3CH_3COCH_3, and **3**·4CH_3COCH_3, **4**·2$(CH_3CH)_2O$, **5**·4$CHCl_3$, and **6**·2CH_3COCH_3·2$CHCl_3$

	1·2CH_3COCH_3·2C_6H_{14}	**2′a**·1.5CH_2Cl_2	**2′b**·3CH_3COCH_3	**3**·4CH_3COCH_3
empirical formula	$C_{64}H_{53}F_{10}Fe_2OPPtTl$	$C_{56.50}H_{39}Cl_3F_{10}Fe_2PPtTl$	$C_{64}H_{54}F_{10}Fe_2O_3PPtTl$	$C_{42}H_{30}F_{10}Fe_2O_2PtTl_2$
fw	1570.21	1556.36	1603.20	1472.19
temp (K)	173(1)	173(1)	173(1)	120(1)
wavelength (Å)	0.71073	0.71073	0.71073	0.71073
cryst syst	triclinic	triclinic	triclinic	monoclinic
space group	$P\bar{1}$	$P\bar{1}$	$P\bar{1}$	$P2_1/n$
a (Å); α(deg)	12.0123(3); 85.944(2)	11.5763(3); 76.9090(10)	11.688; 75.19	12.9838(4); 90
b (Å); β(deg)	12.7334(2); 89.7900(10)	15.0440(7); 87.142(3)	16.063; 70.36	22.8519(6); 99.173(2)
c (Å); γ(deg)	17.5903(5); 78.474(2)	16.6926(8); 80.036(2)	17.105; 76.96	13.5598(2); 90
V (Å^3); Z	2629.56(11); 2	2788.6(2); 2	2889.3; 2	3971.80(17); 4
calcd density (Mg/m^3)	1.874	1.854	1.843	2.462
abs correction (mm^{-1})	6.353	6.133	5.792	12.394
F(000)	1422	1490	1556	2720
cryst size (mm^3)	0.3 × 0.2 × 0.175	1.00 × 0.01 × 0.01	0.10 × 0.10 × 0.10	0.375 × 0.2 × 0.15
2θ range (deg)	3.68−28.13	2.17−26.37	1.93−28.12	2.37−25.68
index ranges	$-15 \le h \le 15$	$-14 \le h \le 14$	$0 \le h \le 15$	$-15 \le h \le 15$
	$-16 \le k \le 16$	$-18 \le k \le 18$	$-19 \le k \le 21$	$-27 \le k \le 27$
	$-22 \le l \le 22$	$-20 \le l \le 20$	$-20 \le l \le 22$	$-15 \le l \le 11$
reflns collected	41496	40340	12965	30402
independent reflns	12440 [R(int) = 0.0680]	11382 [R(int) = 0.0573]	12965 [R(int) = 0.0000]	7138 [R(int) = 0.0567]
data/restraints/params	12440/0/669	11382/1/683	12965/0/737	7138/0/536
goodness of fit on F^{2a}	1.042	1.038	1.030	1.039
final R indices [$I > 2\sigma(I)$] [a]	R1 = 0.0422, wR2 = 0.0984	R1 = 0.0406, wR2 = 0.0952	R1 = 0.0452, wR2 = 0.0873	R1 = 0.0621, wR2 = 0.1539
R indices (all data)[a]	R1 = 0.0675, wR2 = 0.1063	R1 = 0.0585, wR2 = 0.1028	R1 = 0.0792, wR2 = 0.1005	R1 = 0.0788, wR2 = 0.1721
largest diff. peak and hole	1.508 and −1.333 eÅ^{-3}	2.083 and −1.101 e.Å^{-3}	1.511 and −1.556 e.Å^{-3}	2.81 and −3.608 eÅ^{-3}

	4·2$(CH_3CH)_2O$	**5**·4$CHCl_3$	**6**·2CH_3COCH_3·2$CHCl_3$
empirical formula	$C_{44}H_{38}F_{10}Fe_2O_2PtTl_2$	$C_{39}H_{28}Cl_6F_2NPtTl$	$C_{52}H_{43}Cl_3Fe_4OPtTl_2$
fw	1504.27	1234.48	1617.44
temp (K)	173(1)	173(1)	173(1)
wavelength (Å)	0.71073	0.71073	0.71073
cryst syst	triclinic	triclinic	monoclinic
space group	$P\bar{1}$	$P\bar{1}$	$P2_1/n$
a (Å); α (deg)	11.9302(7); 116.619(2)	11.6669(5); 77.775(2)	11.6114(3); 90
b (Å); β (deg)	14.7723(8); 96.068(2)	15.4534(4); 85.428(2)	23.9774(11); 98.230(2)
c (Å); γ (deg)	14.8538(8); 108.888(2)	22.7020(9); 69.481(2)	17.4382(8); 90
V (Å^3); Z	2114.8(2); 2	3746.3(2); 4	4805.0(3); 4
calcd density (Mg/m^3)	2.362	2.189	2.236
abs correction (mm^{-1})	11.641	9.229	10.960
F(000)	1400	2328	3032
cryst size (mm^3)	0.25 × 0.2 × 0.125	0.2 × 0.15 × 0.1	0.10 × 0.10 × 0.05
2θ range (deg)	2.67−26.37	4.09−25.35	2.07−26.37
index ranges	$0 \le h \le 14$	$0 \le h \le 14$	$-10 \le h \le 14$
	$-18 \le k \le 17$	$-16 \le k \le 18$	$-21 \le k \le 29$
	$-18 \le l \le 18$	$-27 \le l \le 27$	$-21 \le l \le 21$
reflns collected	8628	13641	32560
independent reflns	8268 [R(int) = 0.0000]	13641 [R(int) = 0.0000]	9804 [R(int) = 0.0749]
data/restraints/params	8628/0/557	13641/5/889	9804/0/570
goodness of fit on F^{2a}	1.063	1.063	1.017
final R indices [$I > 2\sigma(I)$] [a]	R1 = 0.0392, wR2 = 0.0727	R1 = 0.0448, wR2 = 0.0713	R_1 = 0.0464, wR_2 = 0.0804
R indices (all data)[a]	R1 = 0.0594, wR2 = 0.0799	R1 = 0.0815, wR2 = 0.0826	R_1 = 0.0885, wR_2 = 0.0913
largest diff. peak and hole	1.452 and −1.991 e Å^{-3}	1.474 and −1.342 e Å^{-3}	1.231 and −1.052 e Å^{-3}

[a] $R1 = \sum(|F_o| - |F_c|)/\sum|F_o|$; $wR2 = [\sum w(F_o^2 - F_c^2)^2/\sum wF_o^2]^{1/2}$; goodness of fit $= \{\sum[w(F_o^2 - F_c^2)^2]/(N_{obs} - N_{param})\}^{1/2}$; $w = [\sigma^2(F_o) + (g_1P)^2 + g_2P]^{-1}$; $P = [\max(F_o^2;0) + 2F_c^2]/3$.

solution of the crude compounds. Complex **6** was crystallized by slow diffusion at −30 °C of an acetone solution of $TlPF_6$ into a $CHCl_3$ solution of the precursor $(NBu_4)_2[Pt(C{\equiv}CFc)_4]$. X-ray intensity data were collected with a Nonius κ-CCD area-detector diffractometer, using graphite-monochromated Mo Kα radiation. Images were processed using the DENZO and SCALEPACK[30] programs, carrying out the absorption correction at this point for **2′b**, **4**, and **5**. In the cases of **1, 2′a**, **3**, and **6**, the absorption correction was performed using MULTISCAN.[31] The structures were solved by direct methods (**1, 2′a**, **6**) or Patterson methods (**3**, **4**) using SHELXS-97[32] or SIR2004[33] (**2′b**) or by Patterson and Fourier methods using DIRDIF99[34] (**5**). The structures were

(30) Otwinowski, Z.; Minor, W. In *Methods in Enzymology*; Carter, C. V., Jr., Sweet, R. M., Eds.; Academic Press: New York, 1997; Vol. *276A*, p 307.
(31) Blessing, R. H. *Acta Crystallogr.* **1995**, *A51*, 33–38.
(32) Sheldrick, G. M. *SHELX-97*; University of Göttingen: Göttingen. Germany, 1997.
(33) Burla, M. C.; Caliandro, R.; Camalli, M.; Carrozzini, B.; Cascarano, G. L.; De Caro, L.; Giacovazzo, C.; Polidori, G.; Spagna, R. *J. Appl. Crystallogr.* **2005**, *38*, 381–388.
(34) Beursken, P. T.; Admiraal, G.; Beursken, G.; Bosman, W. P.; García-Granda, S.; Gould, R. O.; Smith, M. M.; Smykalla, C. *The DIRDIF99 program system, Technical Report of the Crystallograpy*; Laboratory at University of Nijmegen, University of Nijmegen: Nijmegen, The Netherlands, 1999.

refined by full-matrix least-squares on F^2 with SHELXL-97.[32] All non-hydrogen atoms were assigned anisotropic displacement parameters, and all hydrogen parameters were constrained to idealized geometries, fixing isotropic displacement parameters of 1.2 times the U_{iso} value of their attached carbon for the aromatic hydrogen atoms and 1.5 for the methyl groups. One, three, or two molecules of acetone; two of diethylether; or 4 molecules of $CHCl_3$ were found in the asymmetric units of **1**, **2′b**, **3**, **4**, and **5**, respectively. For **2′a**, 1.5 molecules of CH_2Cl_2 were found, and planarity and distance restraints for the Cl−C−Cl fragment were used to model the molecule, which has 0.5 occupancy. Also, the anisotropic displacement of C57 was given for C58 (EADP C57, C58). The asymmetric unit of complex **6** reveals the presence of one molecule of acetone interacting with one Tl atom and also with a $CHCl_3$, giving rise to the final formulation of the crystal $\mathbf{6}\cdot 2CH_3COCH_3\cdot 2CHCl_3$. For complex **1**, the program SQUEEZE[35,36] showed the presence of one void of 137 Å^3 in the unit cell containing 53 electrons per asymmetric unit. This fits well with the presence of one molecule of hexane, which has been included in the empirical formula ($C_{55}H_{26}F_{10}Fe_2PPtTl\cdot CH_3COCH_3\cdot C_6H_{14}$). For **3**, the Fourier map at the end of refinement shows some local peaks with large densities (largest 2.81 e Å^{-3}). Inspection of the contoured map using Platon[36] revealed the presence of two small voids of 14 Å^3 per unit cell, insufficient to locate any solvent molecule. As would be expected from the characteristics of that contoured map, an assignment of this electronic density could not be carried out. The results reported here are those obtained from a refinement in which these peaks were not assigned and with no further treatment of data. For **5**, one molecule of $CHCl_3$ showed positional disorder, which was refined over two positions with occupancy factors of 0.75/0.25. Additionally, a cyclopentadienyl ring of one ferrocenyl group was modeled adequately (EADP C28−C32). Finally, in all complexes, some residual peaks bigger than 1 e Å^{-3} were observed close to metal atoms or the solvents, but with no chemical meaning.

Computational Details. All DFT calculations were carried out using the Gaussian 03[37] package. All calculations applied the Becke's three-parameter hybrid function combined with the Lee−Yang−Parr correlation function (B3LYP).[38] The basis set used was the LanL2DZ[39] effective core potential for the metal centers (Pt and Tl) and 6-31G(d,p) for the ligand atoms. The anion [*trans*-$Pt(C_6F_5)_2(C{\equiv}CFc)_2]^{2-}$ was optimized under vacuum conditions, and no negative values were found in the results of the vibrational frequency analysis. Model 1 and Model 2 were constructed by isolating the {(*trans*-$PtTl(C_6F_5)_2(C{\equiv}CFc)_2)^-$} and {*trans*-$PtTl_2(C_6F_5)_2(C{\equiv}CFc)_2$} entities from the X-ray structure obtained for complexes **2′** (Model 1) and **4** (Model 2), since our efforts to obtain an adequate optimized structure were unsuccessful. Single point calculations were performed on complex **3**, Model 1, and Model 2 using the molecular geometry obtained through X-ray diffraction analysis, keeping all distances, angles, and dihedral angles frozen.

Results and Discussion

Synthesis. As shown in Scheme 1, the final structures of the polymetallic Pt−Tl−Fe systems strongly depend on the geometry of the precursor and the Pt/Tl ratio. Thus, by starting from the *heteroleptic cis*-configured precursors [*cis*-$Pt(C_6F_5)_2(C{\equiv}CFc)_2]^{2-}$ and $[Pt(bzq)(C{\equiv}CFc)_2]^-$ (bzq = benzoquinolate), their reactions with 1 equiv of $TlPF_6$ in acetone respectively afford discrete anionic (**1**) and neutral (**5**) octanuclear $Pt_2Tl_2Fe_4$ derivatives, stabilized by both $Pt^{II}\cdots Tl^{I}$ and $Tl^{I}\cdots\eta^2$(alkynyl) bonds. By contrast, the related reaction of [*trans*-$Pt(C_6F_5)_2(C{\equiv}CFc)_2]^{2-}$ with 1 equiv of Tl^+ evolves with the formation of a polymeric anionic 1-D extended complex $[\{trans,trans,trans\text{-}PtTlFe_2\}^-]_n$ (**2**), generated by $Pt^{II}\cdots Tl^{I}$ bonds. In the same way, while total neutralization of [*cis*-$Pt(C_6F_5)_2(C{\equiv}CFc)_2]^{2-}$ with 2 equiv of $TlPF_6$ affords the neutral discrete decanuclear $[\{trans,cis,cis\text{-}PtTl_2Fe_2\}]_2$ (**3**) complex, the unusual polymeric complex $[\{trans,trans,trans\text{-}PtTl_2Fe_2\}]_n$ (**4**), containing both $Pt^{II}\cdots Tl^{I}$ and $Tl^{I}\cdots Tl^{I}$ bonding interactions, is generated from the corresponding platinate(II) [*trans*-$Pt(C_6F_5)_2(C{\equiv}CFc)_2]^{2-}$ precursor. Interestingly, in the final neutral systems **3** and **4**, the incoming Tl^+ is easily removed by the addition of an external Br^- source. Thus, the addition of PPh_3MeBr to **3** and **4** induces the precipitation of TlBr, returning the reaction toward the formation of the anionic derivatives **1** and **2′**, respectively. As expected, the neutral complexes **3** and **4** were also generated by treatment of **1** and **2** or **2′** with the required additional Tl^+. Finally, as is shown in Scheme 1, the reaction of the *homoleptic* [$Pt(C{\equiv}CFc)_4]^{2-}$ with 2 equiv of $TlPF_6$ evolves with a final formation of the tetradecanuclear sandwich type complex [$Pt_2Tl_4(C{\equiv}CFc)_8$] (**6**).

All complexes were isolated as air- and moisture-stable orange solids and were fully characterized by usual analytical and spectroscopic techniques (*vide infra*) as well as single-crystal X-ray crystallography. It should be noted that conductivity measurements (acetone solutions) for **1** and the slope observed for the Onsager eq (964) are typical of 2:1 electrolytes.[40] In agreement with its formulation, however, **2** and **2′** show an equivalent conductivity characteristic to that of a 1:1 electrolyte, indicating that the polymeric chain is broken in solution into monomeric $[PtTl(C_6F_5)_2(C{\equiv}CFc)_2]^-$ fragments. For the neutral complexes **3** and **4**, low values of conductivity were measured (Λ_m; 21.3, **3**; 25.6 $\Omega^{-1}cm^2\,mol^{-1}$, **4**), suggesting some degree of dissociation via breaking of the Pt···Tl bonding interaction, in agreement with NMR studies (*vide infra*). In the case of **6**, its insolubility precludes any study in solution, whereas **5** is only slightly soluble in CH_2Cl_2 and $CHCl_3$, and in these no-donor solvents, it behaves as no conductor.

Crystal Structures. Structures and selected data are given in Figures 1−6 and Table 2. ORTEP views and more detailed distance and angle tables are available in the Supporting Information: Figures S1−S7 and Tables S1−S4. The molecular structures of the *heteroleptic cis*-configured platinum−thallium derivatives **1**, **3**, and **5** reveal that in these complexes, the acidic Tl^{I} centers have a clear preference for metallophilic $6s^2-d^8$ $Tl^{I}\cdots Pt^{II}$ bonding interactions, while the $Tl^{I}\cdots$alkynyl bonding is the driving force for the formation of the final dimers. Thus, the octanuclear *cis*-derivatives **1** and **5** (Figures 1 and 2) are formed by two "$PtTl(C_6F_5)_2(C{\equiv}CFc)_2$" or "$PtTl(bzq)(C{\equiv}CFc)_2$" entities, exhibiting a short $Pt^{II}\cdots Tl^{I}$ bonding interaction [2.9257(3) Å, **1**; 2.8511(5), 2.9135(5) Å, **5**],[24,25,27,41,42] which dimerize to give

(35) van der Sluis, P.; Speck, A. L. *Acta Crystallogr., Sect. A* **1990**, *46*, 194–201.
(36) Speck, A. L. *PLATON*;, Utrecht University: Utrecht, The Netherlands, 2008.
(37) Frisch, M. J. et al. *Gaussian 03*, Revision E.01; Gaussian, Inc.: Wallingford, CT, 2004 (see the Supporting Information for complete citation).
(38) Becke, A. D. *Phys. Rev. A* **1988**, *38*, 3098–3100. Lee, C.; Yang, W.; Parr, R. G. *Phys. Rev. B* **1988**, *37*, 785–789. (c) Becke, A. D. *J. Chem. Phys.* **1993**, *98*, 5648–5652.
(39) Wadt, W. R.; Hay, P. J. *J. Chem. Phys.* **1985**, *82*, 284–298.
(40) Feltham, K. O.; Hayter, R. G. *J. Chem. Soc.* **1964**, 4587–4591.
(41) Falvello, L. R.; Forniés, J.; Garde, R.; García, A.; Lalinde, E.; Moreno, M. T.; Steiner, A.; Tomás, M.; Usón, I. *Inorg. Chem.* **2006**, *45*, 2543–2552. (b) Forniés, J.; García, A.; Lalinde, E.; Moreno, M. T. *Inorg. Chem.* **2008**, *47*, 3651–3660.

Scheme 1

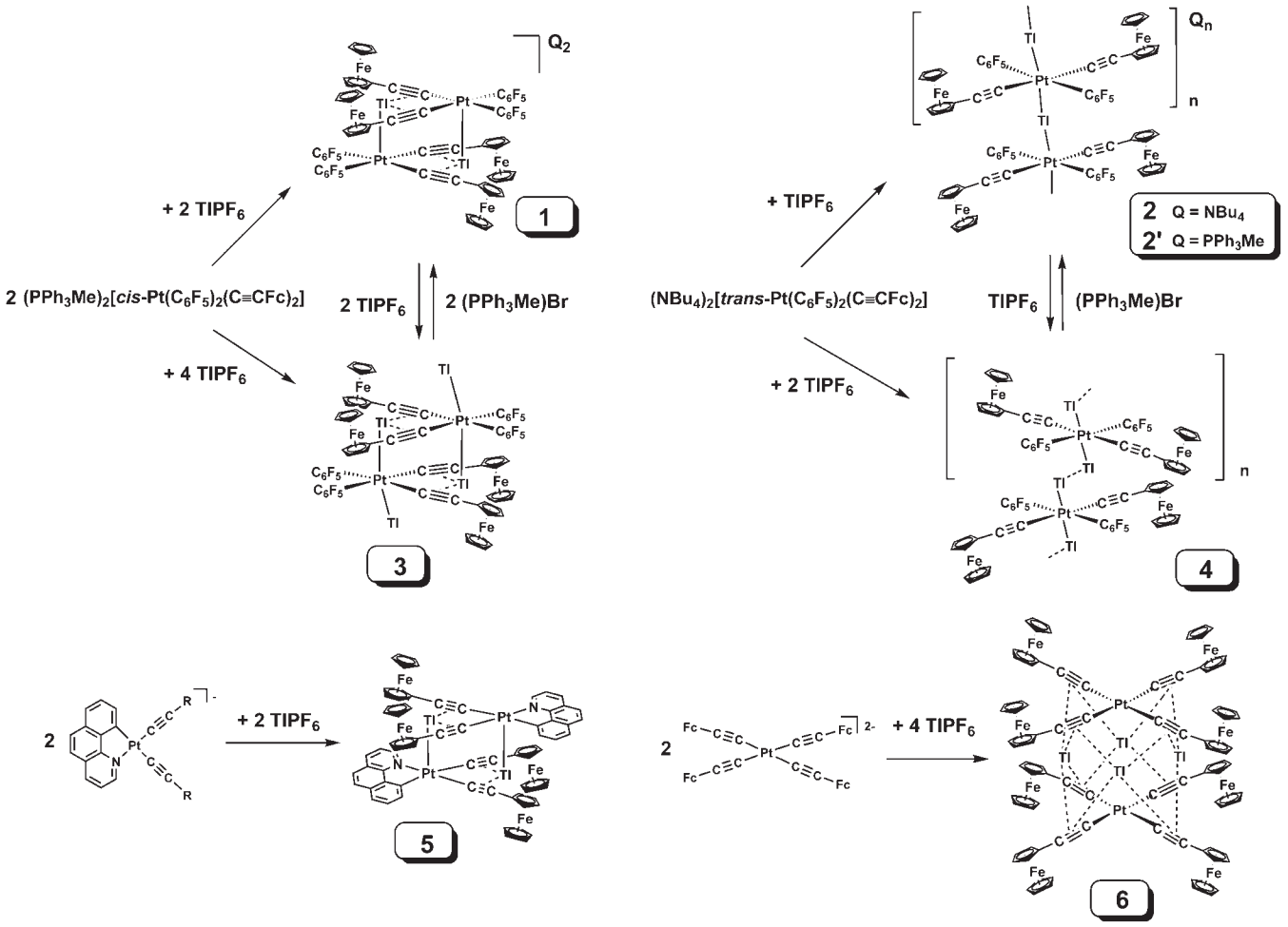

$Pt_2Tl_2Fe_4$ derivatives by η^2 bonding of the Tl^I center of one unit with the acetylenic carbon atoms of both alkynyl fragments of the other unit [Tl···C_α/C_β, 2.956(5)−3.084(5) Å, **1**; 2.919(9)−3.050(9) Å, **5**].[24−27] Additional secondary, very weak Tl···C(Cp) [3.454(5)−3.638(7) Å, **1**; 3.37(1)−3.613(9) Å, **5**] and Tl···$F_o(C_6F_5)$ [3.035(3), 3.386(3) Å, **1**] contacts complete the electronic requirements of the Tl^I, probably reducing the lone pair effect at the thallium centers and also contributing to the final stability of the complexes.

Complex **3** crystallizes from acetone/diethylether as $\mathbf{3}\cdot 4CH_3COCH_3$ containing a $PtTl_2Fe_2$ fragment and two molecules of acetone in the unit cell (Figure S4). The platinum exhibits (Figure 3) a distorted pseudo-octahedral coordination with two strong metallophilic $Pt^{II}\cdots Tl^I$ bonds [Tl−Pt−Tl, 144.11(2)°; Pt−Tl, 3.0307(6), 2.9656(6) Å], and the $PtTl_2Fe_2$ unit also dimerizes through weak $\eta^2\cdots$Tl bonding of the internal Tl(1) center [Tl(1)···C_α/C_β, 2.92(1)−3.08(1) Å] and the contribution of two additional bridging acetone molecules between nonequivalent Tl centers (μ-κ^2O) [Tl(1)···O(1), 2.934(9); Tl(2)′···O(1), 2.856(9) Å]. The two remaining acetone molecules are only bonded to the external Tl(2) centers with a Tl(2)−O(2) distance [2.725(9) Å] slightly shorter than those Tl−μ-O(1) bridging contacts, and all of them are comparable with reported values in other thallium acetone solvate species.[24,27,43] It is worth it to note that the Pt−Tl(1) vector is more perpendicular to the platinate fragment than the Pt−Tl(2) [angles from the normal, 12.1(2)° and 23.9(2)°], allowing Tl(2) to contact weakly with one C_α alkynyl carbon of its own unit [Tl(2)···C(13), 2.92(1) Å]. The coordination spheres of both Tl^I ions are also completed with additional weak contacts with the *ortho*-fluorine atoms of the hanging pentafluorophenyl rings [Tl···F, 3.049(6)−3.230(7) Å]. As can be seen in Figure 3b, the metals of the central Pt_2Tl_4 core are almost coplanar, and it is worth it to note that the separation between the internal equivalent Tl(1) centers [3.9857(7) Å] is close to the van der Waals limit (3.92 Å).

(42) (a) Usón, R.; Forniés, J.; Tomás, M.; Garde, R.; Merino, R. I. *Inorg. Chem.* **1997**, *36*, 1383–1387. (b) Díez, A.; Forniés, J.; Gómez, J.; Lalinde, E.; Martín, A.; Moreno, M. T.; Sánchez, S. *Dalton Trans.* **2007**, 3653–3660. (c) Wu, G.; Wang, D. *J. Cluster Sci.* **2007**, *18*, 406–413. (d) Nagle, J. K.; Balch, A. L.; Olmstead, M. M. *J. Am. Chem. Soc.* **1988**, *110*, 319–321. (e) Stork, J. R.; Olmstead, M. M.; Balch, A. L. *J. Am. Chem. Soc.* **2005**, *127*, 6512–6513. (f) Stork, J. R.; Olmstead, M. M.; Fettinger, J. C.; Balch, A. L. *Inorg. Chem.* **2006**, *45*, 849–857. (g) Balch, A. L.; Rowley, S. P. *J. Am. Chem. Soc.* **1990**, *112*, 6139–6140. (h) Renn, O.; Lippert, B.; Mutikainen, I. *Inorg. Chim. Acta* **1993**, *208*, 219–223. (i) Oberbeckmann-Winter, N.; Braunstein, P.; Welter, R. *Organometallics* **2004**, *23*, 6311–6318. (j) Song, H. B.; Zhang, Z. Z.; Hui, Z.; Che, C. M.; Mak, T. C. W. *Inorg. Chem.* **2002**, *41*, 3146–3154. (k) Quadrelli, E. A.; Davies, J. E.; Johnson, B. F. G.; Feeder, N. *Chem. Commun.* **2000**, 1031–1032. (l) Chen, W.; Liu, F.; Xu, D.; Matsumoto, K.; Kishi, S.; Kato, M. *Inorg. Chem.* **2006**, *45*, 5552–5560.

(43) (a) Fernández, E. J.; López-de-Luzuriaga, J. M.; Monge, M.; Olmos, M. E.; Pérez, J.; Laguna, A. *J. Am. Chem. Soc.* **2002**, *124*, 5942–5943. (b) Fernández, E. J.; López-de-Luzuriaga, J. M.; Olmos, M. E.; Pérez, J.; Laguna, A.; Lagunas, M. C. *Inorg. Chem.* **2005**, *44*, 6012–6018.

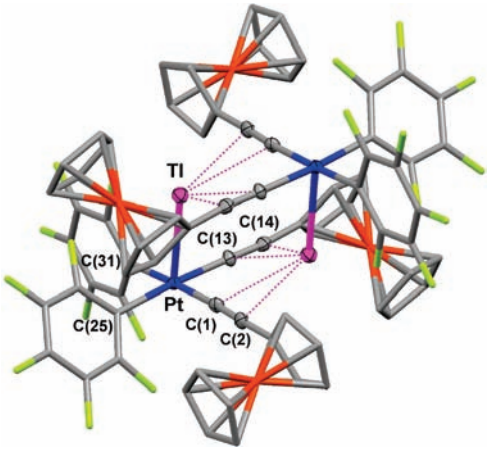

Figure 1. Structure of $\mathbf{1}\cdot 2CH_3COCH_3\cdot 2C_6H_{14}$. Hydrogen atoms, crystallization solvents, and the cations are omitted for clarity. Ellipsoids of metal centers and alkynyl carbons are drawn at the 50% probability level in Figures 1−6.

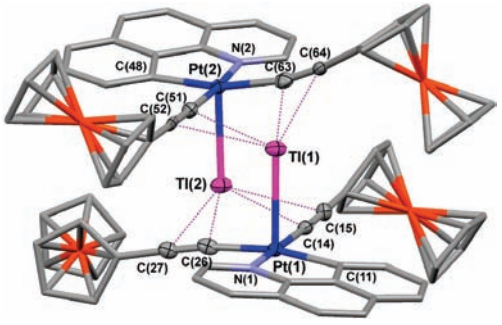

Figure 2. View of the molecular structure of $\mathbf{5}\cdot 4CHCl_3$. Hydrogen atoms, crystallization solvents, and the cations are omitted for clarity.

In contrast to the dimer nature of platinum−thallium heteroleptic *cis* (**1**, **3**, and **5**) derivatives, the *trans*-configured platinum−thallium systems afford extended chains, which are constructed by alternating $[trans\text{-}Pt(C_6F_5)_2(C{\equiv}CFc)_2]^{2-}$ fragments and monovalent Tl^+ ions in **2′a** and **2′b** or divalent $[Tl\cdots Tl]^{2+}$ fragments in **4** (see Figures 4 and 5). Extended networks based on Pt···Tl backbones are not common,[44] and only in rare occasions are these generated by unsupported Pt−Tl bonds.[41] As far as we know, complex **4** is the first reported chain containing the [−Tl···Tl−Pt−Tl···Tl−] sequence as a repeating unit. Interestingly, two forms of crystals of maroon $\mathbf{2'a}\cdot 1.5CH_2Cl_2$ and orange $\mathbf{2'b}\cdot 3CH_3COCH_3$ color, respectively, were formed by varying the solvents of crystallization (see the Experimental Section). In both forms (Figure 4), the anionic $[\{-Pt-Tl-\}^-]_n$ chain adopts a slightly different metallic extended {Pt−Tl−Pt−Tl} conformation, with the crystallographic inversion centers lying on the Tl^I (**2′a**) or the Pt^{II} atoms (**2′b**), respectively. The most significant difference is that in the maroon form, $\mathbf{2'a}^-$, the $Pt^{II}\cdots Tl^I$ distances [Pt(1)−Tl(1)/Tl(2), 2.9565(2), 2.8826(2) Å] are shorter than in the orange form [Pt(1)/Pt(2)−Tl(1), 3.0245(3), 3.0049(2) Å], and the angle Tl(1)−Pt−Tl(2) [164.84(1°)] in $\mathbf{2'a}^-$ is more linear than Pt(1)−Tl(1)−Pt(2) [151.51(1)°] in $\mathbf{2'b}^-$. In both chains, the Tl^I ions display a local octahedral geometry being linked to two Pt−C_α [Tl(1) in $\mathbf{2'a}^-$ and $\mathbf{2'b}^-$] or to two Pt centers [Tl(2) in $\mathbf{2'a}^-$] and to

(44) Akhbari, K.; Morsali, A. *Coord. Chem. Rev.* **2010**, *254*, 1977–2006.

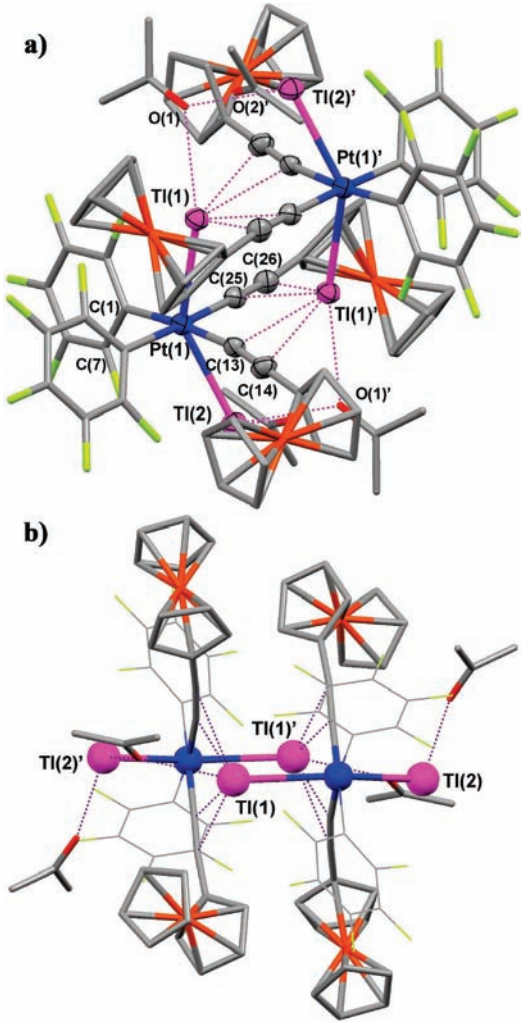

Figure 3. (a) Dimeric disposition of the molecular structure of $\mathbf{3}\cdot 4CH_3COCH_3$. Hydrogen atoms are omitted for clarity. (b) View of the almost coplanar central $[Pt_2Tl_4]$ core.

the four *o*-fluorine atoms of consecutive platinate fragments [2.841(4)−3.119(3) Å]. The cations $[PPh_3Me]^+$ and solvent molecules are located in the corresponding channels formed by four chains, as illustrated in Figure S8.

The *trans*-configured neutral complex **4** crystallizes from acetone/diethyl ether as $[\mathbf{4}\cdot 2(CH_3CH_2)_2O]_n$. Figure 5 illustrates a short (a) and longer (b) section of the unusual extended chain formed by $PtTl_2Fe_2$ units [Pt−Tl 3.0116(3), 3.0169(3) Å], connected through a relatively strong $Tl^I\cdots Tl^I$ [3.6732(5) Å] metallophilic interaction and additional η^2-alkynyl−Tl bonding [Tl···C_α/C_β, 2.958(9)−3.05(1) Å]. The interaction of two Tl^+ centers to form $[Tl\cdots Tl]^{2+}$ has been examined by theoretical calculations.[45] In complex **4**, the Tl(1)···Tl(2) separation [3.6732(5) Å] is comparable to those observed in oligomeric Tl^+ derivatives,[46] or in some recent gold−thallium complexes (3.60−3.70 Å)[43] but longer than distances found in some

(45) Ma, G.; Ferguson, M. J.; Cavell, R. G. *Chem. Commun.* **2010**, *46*, 5370–5372. (b) Janiak, C.; Hoffmann, R. *J. Am. Chem. Soc.* **1990**, *112*, 5924–5946.

(46) For a useful summary of studies of species with Tl···Tl interactions, see: Ghosh, P.; Rheingold, A. L.; Parkin, G. *Inorg. Chem.* **1999**, *38*, 5464–5467.

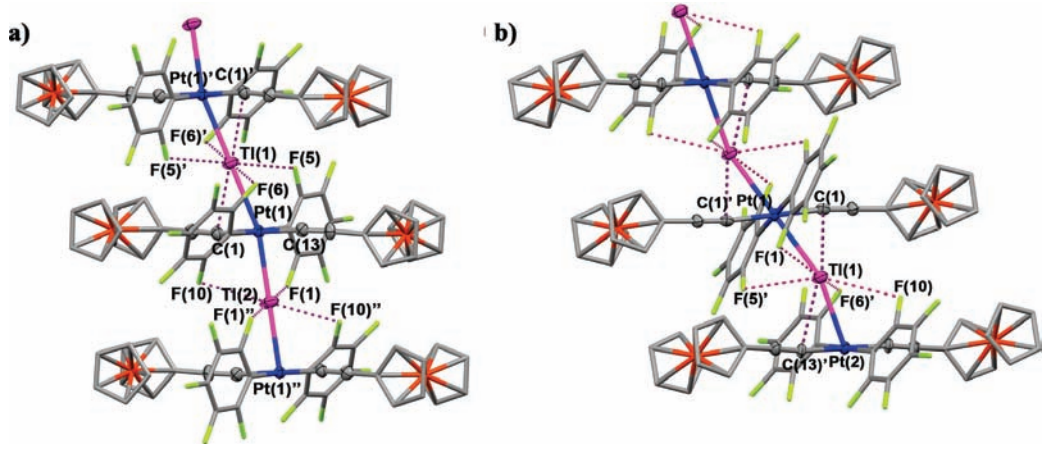

Figure 4. Views of the structure of the anion $\mathbf{2'}^{-}$ in (a) $\mathbf{2'a}\cdot 1.5CH_2Cl_2$, maroon chain; (b) $\mathbf{2'b}\cdot 3CH_3COCH_3$, pale orange chain. Hydrogen atoms, crystallization solvents, and the cations are omitted for clarity.

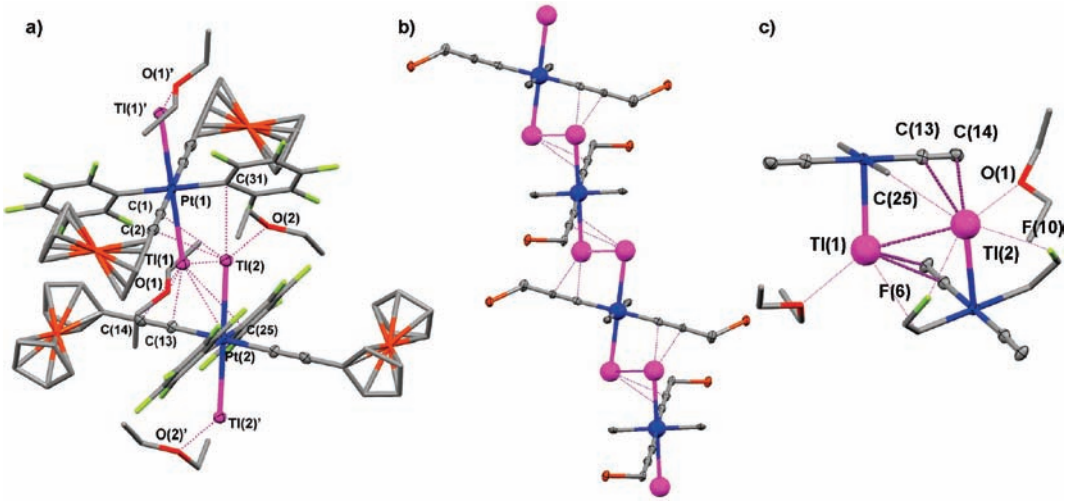

Figure 5. Different views of the molecular structure of $\mathbf{4}\cdot 2(CH_3CH)_2O$. Hydrogen atoms are omitted for clarity. (a) Short section of the extended chain. (b) Longer section of the chain showing the core of metal atoms. (c) Coordination environment for Tl(1) and Tl(2).

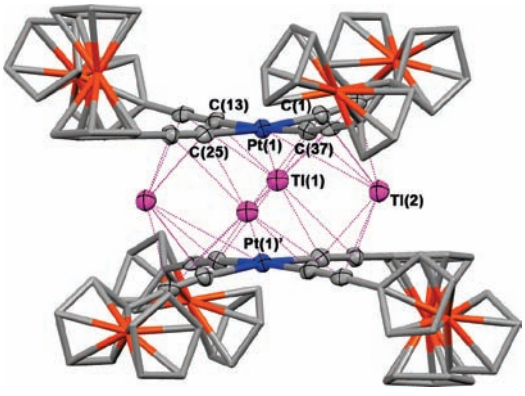

Figure 6. Structure of $\mathbf{6}\cdot 2CHCl_3\cdot 2CH_3COCH_3$. Hydrogen atoms and crystallization solvents are omitted for clarity.

alkyl or aryl thallium(I)[47] derivatives or in Tl metal (3.46 Å).[48] In fact, the extended structure can be alternatively viewed as a continuous chain of slipped and staggered "$[trans\text{-}Pt(C_6F_5)_2(C{\equiv}CFc)_2]^{2-}$" fragments [dihedral angles between consecutive planes 22.3(3)°] linked by a short dicationic $[Tl\cdots Tl]^{2+}$ unit (Figure 5b). Within the binuclear unit, each Tl^{I} completes its coordination (Figure 5c) bonding the oxygen atom of one Et_2O molecule [Tl(1)···O(1), 2.877(5) Å; Tl(2)···O(2), 2.818(7) Å] and with two *ortho*-fluorine contacts [2.840(5)−3.031(7) Å].

Analogously to previously reported homoleptic derivatives $[Pt_2Tl_4(C{\equiv}CR)_8]$ (R = ^{t}Bu, Np),[26,27] in the 14-nuclear aggregate $\mathbf{6}\cdot 2CH_3COCH_3\cdot 2CHCl_3$, the Tl^{I} centers show a stronger preference for the electron-rich alkynyl fragments than for the platinum center, giving rise to a sandwich type structure formed by two eclipsed platinate fragments connected by four thallium centers. Each Tl^{I} center displays a square pyramidal geometry being η^2-bonded to four alkynyl units [Tl···C_α, 2.838(9)−3.044(8) Å; Tl···C_β, 3.066(8)−3.250(9) Å] forming the basal plane with the stereochemically active lone pair at the apex of the pyramid. The central octahedral Pt_2Tl_4 metallic skeleton exhibits a relatively short mutually *trans* Pt···Pt distance of 3.5909(5) Å, which is within the range seen in stacking chain Pt^{II} complexes.[49] This structural feature has also been previously found in other derivatives

(47) (a) Uhl, W.; Keimling, S. U.; Klinkhammer, K. W.; Schwarz, W. *Angew. Chem., Int. Ed.* **1997**, *36*, 64–65. (b) Wright, R. J.; Phillips, A. D.; Hino, S.; Power, P. P. *J. Am. Chem. Soc.* **2005**, *127*, 4794–4799.

(48) Wells, A. F. Structural Inorganic Chemistry. 5th ed.; Clarendon Press: Oxford, U. K., 1984; p 1279.

(49) Gliemann, G.; Yersin, H. *Struct. Bonding* (*Berlin*) **1985**, *62*, 87–153.

Table 2. Selected Distances (Å) and Angles (deg) for Complexes **1**·2CH_3COCH_3·2C_6H_{14}, **2′a**·1.5CH_2Cl_2, **2′b**·3CH_3COCH_3, **3**·4CH_3COCH_3, **4**·2$(CH_3CH_2)_2O$, **5**·4$CHCl_3$, and **6**·2CH_3COCH_3·2$CHCl_3$

	1·2CH_3COCH_3·2C_6H_{14}	**2′a**·1.5CH_2Cl_2	**2′b**·3CH_3COCH_3	**3**·4CH_3COCH_3	**4**·2$(CH_3CH_2)_2O$	**5**·4$CHCl_3$	**6**·2CH_3COCH_3·2$CHCl_3$
Pt−C_α	2.001(6), 2.008(5)	2.013(6), 2.011(6)	2.034(6), 2.016(5)	2.016(12), 2.018(10)	2.014(7), 2.017(8)	1.980(10)−2.027(9)	1.991(9)2−2.005(9)
Pt−C_a	2.072(5), 2.088(5)	2.078(6), 2.102(6)	2.080(6), 2.063(6)	2.068(11), 2.074(11)	2.092(6), 2.098(7)	2.055(8), 2.057(8)	
Pt−N						2.078(7), 2.087(7)	
C_α−C_β	1.208(8), 1.213(8)	1.210(8), 1.208(8)	1.205(8), 1.201(8)	1.192(16), 1.239(16)	1.205(9), 1.205(10)	1.185(12)−1.210(11)	1.207(11)−1.230(11)
Pt−Tl	2.9257(3)	2.9565(2), 2.8826(2)	3.0245(3), 3.0049(2)	2.9656(6), 3.0307(6)	3.0116(3), 3.0169(3)	2.8511(5), 2.9135(5)	3.5077(5)−3.7538(5)
Tl···C_α	2.997(5), 3.084(5)	3.015(6), 3.216(6)	2.936(7), 2.995(8)	2.92(1)−3.08(1)	2.981(9), 3.010(8)	2.919(9)−2.985(7)	2.838(9)−3.044(8)
Tl···C_β	2.956(5), 3.019(6)			2.95(1), 3.02(1)	2.958(9), 3.05(1)	2.988(8)−3.050(9)	3.066(8)−3.250(9)
Tl−Tl	4.0271(3)			3.9857(7), 4.2815(6)	3.6732(5)	4.3221(6)	4.4136(5), 4.5076(5)
Tl···O				Tl(1)−O(1) 2.934(9) Tl(2)−O(2) 2.725(9) Tl(2)′−O(1) 2.856(9)	Tl(1)−O(1) 2.877(5) Tl(2)−O(2) 2.818(7)		Tl(2)−O(1) 3.291(9)
Pt−C_α−C_β	176.6(5), 178.8(5)	174.4(5), 170.2(6)	173.3(5), 173.6(5)	171.2(9), 177.3(10)	177.8(7), 177.1(6)	166.7(7)−178.1(7)	173.2(8)−176.1(7)
C_α−C_β−C_γ	174.4(6), 177.5(6)	179.3(8), 177.2(7)	176.7(7), 178.6(6)	173.4(12), 174.9(13)	178.1(8), 179.1(9)	171.2(10) −179.9(11)	175.4(3)−177.0(9)
Tl−Pt−Tl		164.84(1)	180.0	144.11(2)	180.0		120.67(1), 120.84(1)

$[Pt_2Tl_4(C{\equiv}CR)_8$; 3.572(2)−3.622(5) Å, R = Bu^t, Np].[26,27] The $Pt^{II}\cdots Tl^I$ distances [3.5077(5)−3.7538(5) Å] are only close to the sum of the van der Waals radii of Tl (1.96 Å) and Pt (1.75 Å), indicating the presence of weak heterometallic interactions.[24,25,27,41,42]

In all of these complexes, the Cp rings of the Fc groups are not coplanar with the corresponding coordination planes. The angles are in the range 34.0 to 88.7° for the *cis*-configured **1**, **3**, and **5** and 56.0° to 87.7° in the extended chain *trans*-derivatives **2′** and **4**. In **6**, the peripheral Fc groups form dihedral angles of 13.2°, 57.7°, 63.3°, and 86.0° with the platinum coordination plane. It is worth noting than in **5** the molecules expand to an extended network due to close $\pi\cdots\pi$ intermolecular contacts (*ca.* 3.29−3.38 Å) between the planar benzoquinolate groups of neighboring $Pt_2Tl_2Fe_4$ units (see the Supporting Information, Figure S9).

Spectroscopic Characterization. The IR spectra exhibit characteristic ν(C≡C) absorptions bands (2113−2072 cm^{-1}), which are slightly shifted to higher energy in relation to those seen in the corresponding precursors [ν(C≡C) 2094−2073 cm^{-1}]. This spectroscopic feature has been previously attributed[26,27] to the formation of the $Pt^{II}\cdots Tl^I$ bonding interactions, which decrease somewhat the π-back-donor component (Pt→π*C≡CR) and also to the small covalent contribution associated with the η^2-alkynyl···Tl bonding. The proton spectra of **1**−**5** reflect the interaction of the Tl^I center with the platinum fragments. In particular, the proton resonances of the C_5H_4 rings are systematically shifted to higher frequencies in relation to the corresponding precursor in the same solvent (CD_3COCD_3, **1**−**4**; $CDCl_3$, **5**). The *cis* derivatives **1** and **3** show a higher shift with respect to $(PPh_3Me)_2$[*cis*-$Pt(C_6F_5)_2(C{\equiv}CFc)_2$] (Figure S10a) than the *trans* derivatives **2** and **4** with respect to its precursor $(NBu_4)_2$[*trans*-$Pt(C_6F_5)_2(C{\equiv}CFc)_2$] (Figure S10b). This pattern could be related to the presence in solution of monomeric (**2**, **4**) or dimeric (**1**, **3**) entities, respectively.

In the same way, the ^{19}F NMR studies of **1**−**4** confirm the linkage of Tl^I to the Pt^{II} fragments and the extent of the Tl···*ortho*-fluorine bonding interactions. As an illustration, the variable temperature NMR spectra of complexes **1** and **3** in the *ortho*-fluorine region are shown in Figure 7. As expected, only one set of C_6F_5 signals is seen for all complexes. At low temperatures, the anionic complexes (**1** and **2**/**2′**) exhibit the expected pattern for a rigid fragment $\{[PtTl(C_6F_5)_2(C{\equiv}CFc)_2]^-\}_n$ (n = 2, **1**; 1, **2**, **2′**) with the Tl^I interacting with two *o*-fluorine atoms, one from each static C_6F_5 ring (*o*-F_{endo} in Figure 7a), giving rise to two distinct *o*-F and *m*-F (endo and exo) resonances. The *o*-F_{endo} atoms appear as an extensive doublet due to a short contact $^{203,205}Tl-^{19}F$ coupling in both complexes (∼3300 Hz, **1**; ∼3215 Hz, **2**), with broadened platinum satellites in **1** ($^3J_{o\text{-}F_{endo}\text{-}Pt}$ ∼ 230 Hz). The exo *o*-fluorine atoms are seen in **1** (Figure 7a) as a clear doublet resulting from long-range thallium coupling ($^4J_{F_{exo}\text{-}Tl}$ ∼ 95 Hz) with platinum satellites ($^3J_{F_{exo}\text{-}Pt}$ ∼ 355 Hz) and as a broad singlet in **2** (see the Experimental Section for details). By increasing the temperature, the exo and endo fluorine resonances broaden, coalesce, and finally average to only a singlet signal at higher temperatures, implying that a dynamic behavior is occurring. The last of the thallium−fluorine coupling may be attributed to a fast exchange likely involving a reversible breaking/forming of the Pt−Tl bond, and the observation of higher coalescence temperature for the *cis* configured complex **1** (*o*-F $T_{coalescence}$ ∼ 260 K, **1**, vs $T_{coalescence}$ ∼ 223 K, **2**) could be related to the presence of a more rigid dimer structure for complex **1** in solution (Scheme 1). Interestingly, in complex **3**, the presence of nonequivalent thallium centers (internal and external) is reflected in the coupling constants. Thus, in the *ortho*-fluorine region, the averaged signal observed at room temperature for the *o*-F atoms coalesces at *ca* 240 K, being resolved in the slow regime into two nearly isochronous (endo and exo) fluorine resonances with different splitting patterns (Figure 7b). A doublet with strong coupling to thallium [δ −107.6, $J_{Tl(1)\text{-}Fo}$ = 3618 Hz, $^3J_{Pt-Fo}$ ∼ 220 Hz, endo-F*o*] is assigned, by comparison with the pattern of **1**,

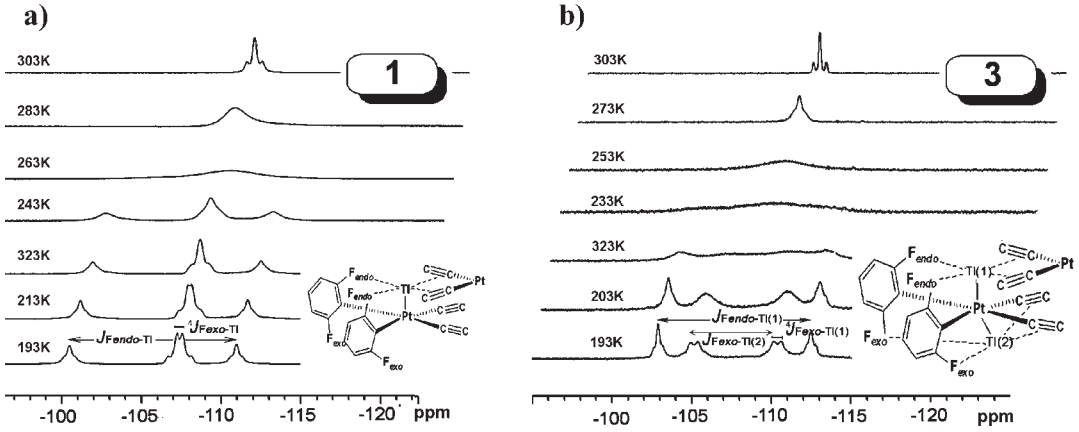

Figure 7. Variable-temperature ^{19}F NMR in CD_3COCD_3 in the *o*-fluorine region of (a) **1** and (b) **3**.

Table 3. Electrochemical Data for Complexes **1**−**5** and Their Corresponding Precursors[a]

	$E_{1/2}$(V) CH_2Cl_2	$E_{1/2}$(V) THF	K_c
Fc/Fc^+	0.46	0.60	
$(PPh_3Me)_2$[*cis*-$Pt(C_6F_5)_2(C{\equiv}CFc)_2$], **A**	0.11, 0.22[b]	0.26, 0.36[b]	
$(NBu_4)_2$[*trans*-$Pt(C_6F_5)_2(C{\equiv}CFc)_2$], **B**	0.08, 0.22[b]	0.24, 0.37[b]	
(NBu_4)[$Pt(bzq)(C{\equiv}CFc)_2$], **C**	0.18, 0.28[b]		40
$(PPh_3Me)_2$[{*trans*,*cis*,*cis*-$PtTl(C_6F_5)_2(C{\equiv}CFc)_2$}$_2$], **1**	0.34[b]	0.44[b]	
[(NBu_4)}*trans*,*trans*,*trans*-$PtTl(C_6F_5)_2(C{\equiv}CFc)_2$}$]_n$, **2**	0.27, 0.37	0.37, 0.47	40
[*trans*,*cis*,*cis*-$PtTl_2(C_6F_5)_2(C{\equiv}CFc)_2]_2$, **3**	0.37	0.54[c]	
[*trans*,*trans*,*trans*-$PtTl_2(C_6F_5)_2(C{\equiv}CFc)_2]_n$, **4**		0.39, 0.47	22
[$PtTl(bzq)(C{\equiv}CFc)_2]_2$, **5**	0.45[b]		

[a] All measurements were carried out at 25 °C with 0.1 M NBu_4PF_6. Scan rate 100 mV s^{-1} and vs Ag/AgCl reference electrode. [b] Together with other waves due to electrogenerated byproduct. [c] E_{pa}.

to the internal or endo-fluorine resonances and a doublet of doublets due to short- [$^3J_{Tl(2)\text{-}Fo} = 1970$ Hz] and long-range [$^4J_{Tl(1)\text{-}Fo} = 175$ Hz] coupling to both thallium centers, with the ^{195}Pt satellites merely visible ($^3J_{Pt-Fo} \sim 367$ Hz), which is therefore attributed to the external or exo-fluorine atoms. The observation of long-range $^4J_{Tl1-Fo}$ only for the exo-*ortho*-fluorine atoms is not common,[50] and it could be attributed to the better overlap between the internal Tl(1) (6s $6p_z$) and the Pt^{II} ($5d_z^2$ $6p_z$) orbitals than between the external Tl(2) and Pt ones. In fact, as commented upon before, in the X-ray structure of **3**, the Pt−Tl(2) vector displaces from the normal to the platinate fragment more than the Pt−Tl(1) [23.9(2)° vs 12.1(2)°]. As seen in **1** and **2**, the lack of $^{203,205}Tl-{}^{19}F$ coupling at higher temperatures could be attributed to a partial dissociation, also supported by the low values of conductivities seen in acetone (Λ_M, 21 $\Omega^{-1}cm^2$ mol^{-1}, **3**), which facilitates fast exchange between the nonequivalent thallium centers. Compound **4** displays a very sharp doublet (δ −107.5, $J_{F-F} \sim 28$ Hz) with ^{195}Pt satellites even at room temperature. By lowering the acquired temperature, both the *o*-F and *m*-F broaden but do not resolve, indicating the occurrence of dynamic behavior even at low temperatures. It should be noted that, although in all these systems (**1**−**4**) partial dissociation of Tl^I is suggested, the occurrence of a simultaneous rotation of the C_6F_5 ring around the Pt−C_{ipso} bonds cannot be completely excluded. However, in both geometries the coalescence temperature for the *ortho*-fluorine atoms decreases by increasing the Tl/Pt ratio (*o*-F $T_{coalesc}$ **2** > **4** and **1** > **3**), suggesting the remarkable role of the reversible breaking/forming of the Pt−Tl bonds, which is more favored in the final neutral complexes.

Electrochemistry. In an attempt to elucidate the effect produced by the interaction of the Tl^I centers with the ferrocenylacetylide platinate fragments, we decided to carry out electrochemical studies. Unfortunately, the insolubility of [$Pt_2Tl_4(C{\equiv}CFc)_8$] (**6**) precludes carrying out its electrochemical study. For complexes **1**−**5**, the redox behavior was investigated by cyclic voltammetry (CV) and differential pulse voltammetry (DPV) techniques. All measurements were carried out in CH_2Cl_2 and THF, except for complexes **4** and **5**, which are insoluble in CH_2Cl_2 and THF, respectively. Cyclic voltammograms of all complexes are given in the Supporting Information (Figures S11−S15), and the most relevant data are summarized in Table 3. For comparison purposes, the previously reported data of the anionic bis(ferrocenylacetylide)platinate(II) precursors together with the Fc/Fc^+ redox couple are also included in Table 3. We note that all anionic [*cis*-$Pt(C_6F_5)_2(C{\equiv}CFc)_2]^{2-}$ (**A**), [*trans*-$Pt(C_6F_5)_2(C{\equiv}CFc)_2]^{2-}$ (**B**), and $[Pt(bzq)(C{\equiv}CFc)_2]^-$ (**C**) precursors display, in addition to two ill resolved waves (0.08−0.18/0.22−0.28 V) due to the oxidation of the Fc groups, other waves where the origin was attributed to byproducts formed after the oxidation of both Fc moieties. The electrochemical study of the [$Pt-Tl_x-(Fc)_2$] ($x = 1, 2$) systems reveals that, in general, partial (complexes **1**, **2**) or total (complexes **3**−**5**) neutralization of the anionic fragments increases the stability of the full oxidized species. On the other hand, the observed $E_{1/2}$ (Fc) values are higher than the values reported for the precursors and also increase with the number of $Pt^{II}\cdots Tl^I$ bonding

(50) Stanek, K.; Czarniecki, B.; Aardoom, R.; Rüegger, H.; Togni, A. *Organometallics* **2010**, *29*, 2540–2546.

interactions, a trend presumably related to the occurrence of an electron-withdrawing effect of the coordinated Tl^I ions, which probably reduces the π-back-donor component from the Pt atom to the ferrocenylethynyl fragments [Pt→π*(C≡CFc)].

Thus, the CV and DPV of the *trans* configured anionic $[\{PtTlFc_2\}^-]_n$ (**2**) and neutral $[PtTl_2Fc_2]_n$ (**4**) species show (Figures S11 and S12), on sweeping at anodic potentials, two reversible and sufficiently well resolved waves corresponding to the successive oxidation of both ferrocenyl groups of the $[trans\text{-}PtTl_x(C_6F_5)_2(C{\equiv}CFc)_2]^n$ unit ($x = 1$, $n = -1$, **2**; $x = 2$, $n = 0$, **4**). Compared to the dianionic precursor, the values of the oxidation potentials of the monoanionic complex $[trans\text{-}PtTl(C_6F_5)_2(C{\equiv}CFc)_2]^-$ ($\mathbf{2}^-$) increase remarkably in both solvents. However, this effect is clearly attenuated on going to the final neutral product [*trans*,*trans*,*trans*-$PtTl_2(C_6F_5)_2(C{\equiv}CFc)_2$] (**4**) THF, $E_{1/2}$ = 0.24 and 0.37 V, **B**, vs 0.37 and 0.47 V, **2**, and 0.39 and 0.47 V, **4**). Interestingly, the electronic interaction between the Fc groups also decreases following the same trend: $\Delta E_{1/2}$ = 0.14 V, **B** > 0.10 V, **2** > 0.08 V, **4**. Both features could be attributed to the formation of the $Pt^{II}\cdots Tl^I$ bonds, which reduces the extent of the Pt(dπ)$\cdots\pi$C(sp) overlap along the chain C≡C−Pt−C≡C and as a consequence the electronic communication between the Fc groups.

In the same way, compared to the *cis*-configured anionic precursors **A** and **C**, which show waves due to electrogenerated byproducts even at a low temperature (−78 °C), the anionic $(PPh_3Me)_2[\{trans,cis,cis\text{-}PtTl(C_6F_5)_2(C{\equiv}CFc)_2\}_2]$, **1** and neutral $[PtTl(bzq)(C{\equiv}CFc)_2]_2$ (**5**) complexes undergo at a low temperature (−78 °C, see Figures S13b and S14b) a single reversible wave attributed to the oxidation of all Fc groups, which is also found at significantly higher potentials (CH_2Cl_2, 25 °C, 0.34 V, **1**; 0.45 V, **5**) than those of **A** and **C**, indicating direct influence of the presence of the $Pt^{II}\cdots Tl^I$ and $Tl^I\cdots$alkynyl bonding interactions. It should be noted that at room temperature both complexes exhibit also additional small features at higher potentials (see Figures S13a and S14a), indicating that the stability of the oxidized species is remarkably lower than that found in the related *trans* complexes **2** and **4**. The neutral complex [*trans*,*cis*,*cis*-$PtTl_2(C_6F_5)_2(C{\equiv}CFc)_2]_2$ (**3**) has only one reversible redox step in CH_2Cl_2 at 25 °C at 0.37 V (Figure S15), which is seen as quasi-reversible or reversible at a low temperature (−78 °C) and shifted to a higher potential in THF (E_{pa} 0.54 V). The difference observed with the solvents could be attributed to their different coordination abilities, but the effect of the solvent could be much more complex.[51] It should be noted that for all of these *cis*-configured complexes, **1**, **3**, and **5**, although the stability of the full oxidized species clearly increases, the small electronic communication observed between the Fc groups in the precursors **A** and **C** however seems to be essentially lost upon Tl^I coordination.

Spectroelectrochemistry. The extent of electronic communication between electroactive groups is currently being studied by spectroelectrochemical (SEC) techniques.[52] Of particular interest for this work are the studies on complexes containing a Pt atom intercalated between two C≡C−Fc groups [$PtL_2(C{\equiv}C{-}Fc)_2$] as different outcomes have been reported for these complexes. Rapenne et al.[53] have shown in a SEC measurement of [*trans*-$Pt(PEt_3)_2(C{\equiv}CFc)_2$] the existence of an intervalence-charge transfer (IVCT) band, proving some interaction between the remote ferrocenyl groups. Curiously, Lang et al.[5] have recently published a SEC measurement of the related [*trans*-$Pt(PPh_2C{\equiv}CFc)_2(C{\equiv}CFc)_2$] without finding any evidence of interaction between the ferrocenylethynyl groups. In order to gain insight into the electronic coupling of the ferrocenylethynyl groups in Pt^{II} complexes, we have carried out *in situ* spectroelectrochemical measurements of the *trans*-configured complexes **2** and **4** and the neutral *cis*-configured complex **3**, which have shown a marked stability of their oxidized forms. Representative spectra obtained in the SEC experiments are depicted in Figure 8 for **2** and in the Supporting Information (Figures S16 and S17, for **3** and **4**). The UV-vis-NIR spectra of all complexes in CH_2Cl_2 for **2** and **3** and in THF for **4** show a low-energy band (465, **2**; 460, **3**; 480 nm, **4**) which is attributed, according to previous assignments,[4] to an MLCT transition from the ferrocenylethynyl units (−C≡CFc), with some d−d character. In accordance with the electrochemical results, the *cis*-configured complex [*trans*,*cis*,*cis*-$PtTl_2(C_6F_5)_2(C{\equiv}CFc)_2]_2$ (**3**) shows no evidence of any IVCT band (Figure S16). Thus, the gradual oxidation of the Fc groups only produces the apparition of a low energy band at 960 nm, which increases its intensity upon full oxidation.

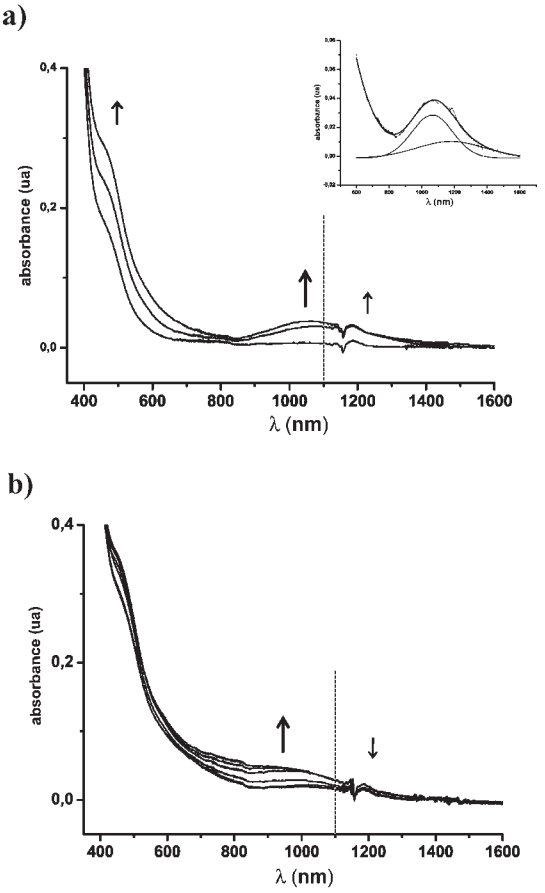

Figure 8. Spectroscopic changes upon oxidation of the first (a) and the second (b) ferrocenyl groups of **2** in CH_2Cl_2 in an OTTLE cell.

(51) Zanello, P. *Inorganic Electrochemistry. Theory, Practice and Application*; The Royal Society of Chemistry: Cambridge, U. K., 2003.

(52) (a) Kaim, W.; Klein, A. *Spectroelectrochemistry*; The Royal Society of Chemistry: Cambridge, UK, 2008. (b) Kaim, W.; Fiedler, J. *Chem. Soc. Rev.* **2009**, *38*, 3373–3382.

(53) Vives, G.; Carella, A.; Sistach, S.; Launay, J. P.; Rapenne, G. *New J. Chem.* **2006**, *30*, 1429–1438.

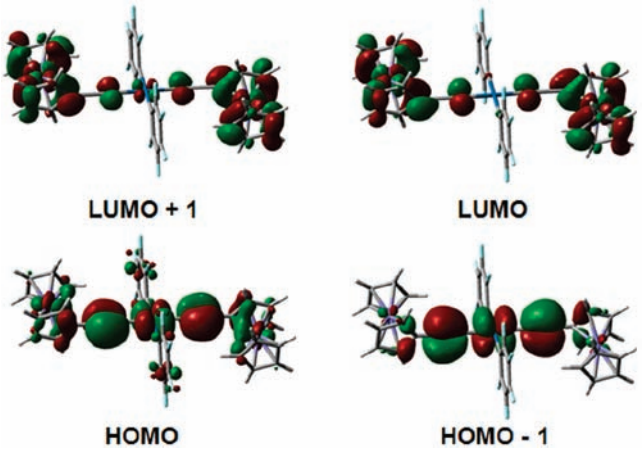

Figure 9. Frontier molecular orbitals obtained from DFT for [*trans*-$Pt(C_6F_5)_2(C{\equiv}CFc)_2]^{2-}$.

This band is attributed, following previous assignments,[18,54] to a metal-to-metal charge transfer MMCT from the Pt−C≡C unit to the ferrocenium fragment.

By contrast, the spectroelectrochemistry of the *trans*-configured derivatives **2** and **4** display a clearly different pattern. Due to the small splitting between both half-wave potentials ($\Delta E_{1/2}$ = 0.10 V, $K_c \sim 40$, **2**; $\Delta E_{1/2}$ = 0.08 V, $K_c \sim 22$, **4**), the analysis of the electronic spectra of their oxidized species is complicated, since during the oxidation mixtures of mixed valence and totally oxidized complexes are easily formed.[55] In both complexes, oxidation of one ferrocenyl group in CH_2Cl_2 for **2** and in THF for **4** produces the gradual growth of a broad low-energy band centered at *ca.* 1050 and 1100 nm for **2** and **4**, respectively (Figure 8a and Figure S17a), which could be explained as a superposition of two overlapped Gaussian-shape bands with maxima at 1065 and 1185 nm for **2** (inset Figure 8a) and at 1069 and 1250 nm (inset, Figure S17a) in the case of the neutral complex **4**. The high-energy band (1065, **2**; 1069 nm, **4**) is attributed to a MMCT from the Pt−C≡C fragment to the ferrocenium subunit, while the lower energy band (1185, **2**; 1250 nm, **4**) could be tentatively ascribed to the presence of an IVCT band in the mixed-valence species. In accordance with this suggestion, further oxidation of the second ferrocenyl group causes the disappearance of the IVCT band (Figures 8b and S17b), thus confirming some electronic interaction between the ferrocenyl groups, and produces a blue-shift of the MMCT band to 960 nm for **2** and 1040 nm for **4**. Similar blue-shifts have been previously observed[5] and have been attributed to the lowering of the Pt−C≡C orbitals after the oxidation of the second ferrocenyl group.

Computational Studies. DFT calculations were performed on the anion of the precursor [*trans*-$Pt(C_6F_5)_2(C{\equiv}CFc)_2]^{2-}$ (**B**), complex **3**, and also on fragments {(*trans*-$PtTl(C_6F_5)_2(C{\equiv}CFc)_2)^-$} Model 1, and {*trans*-$PtTl_2(C_6F_5)_2(C{\equiv}CFc)_2$} Model 2 as adequate models for complexes **2** and **4** in solution. Contour plots of the corresponding frontier molecular orbitals are shown in Figures 9 and S18 (**B**), S19 (Model 1), S20 (Model 2), and S21 (**3**). The dianionic [*trans*-$Pt(C_6F_5)_2(C{\equiv}CFc)_2]^{2-}$ was fully optimized without symmetry restrictions. For complexes **3**, Model 1 {$PtTl(C_6F_5)_2(C{\equiv}CFc)_2)^-$} and Model 2 {$PtTl_2(C_6F_5)_2(C{\equiv}CFc)_2$}, the geometries were taken from the corresponding crystal structures. In the cases of Model 1 and Model 2, they were constructed breaking the extended chains obtained from the X-ray structures for **2** and **4**, respectively.

As shown in Figure 9, the frontier orbitals (HOMO−1 to LUMO+1) computed for the dianionic [*trans*-$Pt(C_6F_5)_2(C{\equiv}CFc)_2]^{2-}$ precursor are mostly contributed by the Fc−C≡C−Pt−C≡C−Fc fragment, suggesting, as shown in previous theoretical studies of other [*trans*-$PtL_2(C{\equiv}CFc)_2$] systems,[53] that there is a possible path for the electronic communication between the Fc groups. The formation of the $Pt^{II}\cdots Tl^{I}$ bonds causes a remarkable modification on the lower unoccupied orbitals, which now have strong contributions from the thallium orbitals (see Figures S19−S21). However, for both systems (Model 1 and Model 2), the HOMO is rather similar to that of the precursor (Figures S19 and S20), having contributions from both Fc groups and the C≡C−Pt−C≡C bridge. This result contrasts with the nature of the frontier orbitals found for *cis*-configured {$PtTl_2Fe_2$}$_2$ (**3**). As is shown in Figure S21, any of the frontier orbitals are delocalized through the C≡C−Pt−C≡C fragment. LUMO to LUMO+3 are mostly contributed form Tl and Pt orbitals, whereas HOMO to HOMO−3 are mainly located on discrete Fc groups. These results lend further support to the experimental data, which indicate some degree of electronic communication between the Fc groups in *trans*-configured complexes **2** and **4**.

Conclusions. High nuclearity Pt−Tl−Fe derivatives containing C≡CFc ligands have been synthesized by neutralization of anionic *heteroleptic* ([*cis*/*trans*-$Pt(C_6F_5)_2(C{\equiv}CFc)_2]^{2-}$, $[Pt(bzq)(C{\equiv}CFc)_2]^-$) or *homoleptic* ($[Pt(C{\equiv}CFc)_4]^{2-}$) ferrocenylethynylplatinate(II) precursors with Tl^+ and have been structurally and spectroscopically characterized. The *cis*-configured platinate precursors generate discrete high-nuclearity systems [octanuclear $[PtTlFe_2]_2$ (**1**, **5**) and decanuclear $[PtTl_2Fe_2]_2$ (**3**)] based on heterometallic units with strong metallophillic $Pt^{II}\cdots Tl^{I}$ bonding interactions, which dimerize by $Tl^{I}\cdots\eta^2$(alkynyl) interactions. However, the *trans* platinate precursor [*trans*-$Pt(C_6F_5)_2(C{\equiv}CFc)_2]^{2-}$ produces rare examples of one-dimensional chain materials, based on $Pt^{II}\cdots Tl^{I}$ metallophilic backbones, constructed by alternating *trans*-platinate(II) fragments and Tl^+ ions (**2′a**, **2′b**) or divalent $[Tl\cdots Tl]^{2+}$ units (**4**). In the case of the *homoleptic* $[Pt(C{\equiv}CFc)_4]^{2-}$ complex, the thallium centers exhibit a bonding preference for the electron-rich alkyne entities to give rise the tetradecanuclear $[Pt_2Tl_4Fe_8]$ sandwich-type derivative.

Electrochemical studies have been carried out for the *cis*- (**1**, **3**, and **5**) and *trans*-configured (**2**, **4**) systems. These studies have shown that the Tl^{I} coordination to the ferrocenylethynyl platinum(II) fragments clearly increases the stability of the full oxidized species, this effect being more remarkable in the *trans*-configured systems **2** and **4**. In addition, the formation of $Pt^{II}\cdots Tl^{I}$ bonds reduces the available electronic density on the Fc−C≡C−Pt−C≡C−Fc fragments, causing in all systems (**1**−**5**) an anodic shift in the oxidation potential of the Fc groups, which increases with the Tl/Pt ratio. The observed anodic shift is higher in the *cis*-configured complexes (**1**, **3**, and **5**) likely due to the presence of a secondary $Tl^{I}\cdots\eta^2$-alkynyl, which stabilizes the dimer

(54) (a) De Biani, F. F.; Manca, G.; Marchetti, L.; Leoni, P.; Bruzzone, S.; Guidotti, C.; Atrei, A.; Albinati, A.; Rizzato, S. *Inorg. Chem.* **2009**, *48*, 10126–10137. (b) Sato, M.; Mogi, E.; Katada, M. *Organometallics* **1995**, *14*, 4837–4843.

(55) Richardson, D. E.; Taube, H. *Coord. Chem. Rev.* **1984**, *60*, 107–129.

entities in solution, also supported by NMR spectroscopy. In the same way, upon Tl^{I} coordination, the observed electronic interaction between the Fc groups decreases, being essentially lost for the *cis*-configured complexes **1**, **3**, and **5**. In the *trans*-configured derivatives (**2** and **4**), the Fc groups still display some degree of communication, as suggested by CV and DPV ($\Delta E_{1/2}$, 0.10 V, **2**; 0.08 V, **4**) and also supported by the presence of an IVCT band in their UV−vis−NIR spectra of oxidized compounds and comparative DFT calculations.

Acknowledgment. This work is dedicated to Prof. María Teresa Chicote on the occasion of his 60th birthday. This work was supported by the Spanish MICINN (Project CTQ2008-06669-C02-02/BQU and a grant for A.D.). J.F. thanks the CAR (COLABORA project 2009/05), and S.S. thanks the CSIC for a grant. The authors also gratefully acknowledge the research group of Prof. J. A. Palacios of the Universidad de Burgos for their help and fruitful discussions in spectroelectrochemistry. We also thank CESGA for computer support.

Supporting Information Available: ORTEP views of the asymmetric unit of complexes **1**−**6** (Figures S1−S7). Packing diagram of **2′a** and **2′b** (Figure S8). Crystal packing of **5** (Figure S9). Comparative ferrocenyl region of the ^{1}H NMR spectra of **3** and **1** and **4** and **2** vs their corresponding precursors (Figure S10). CV of **2** in CH_2Cl_2 at 25 °C (Figure S11). DPV and CV of **4** in CH_2Cl_2 at 25 °C (Figure S12). CV of **1** in THF and **5** in CH_2Cl_2 at 25 °C and at −78 °C (Figures S13 and S14). CV of **3** in CH_2Cl_2 at 25 °C (Figure S15). SEC of **3** in CH_2Cl_2 and **4** in THF (Figures S16 and S17). Computed frontier molecular orbitals for $[trans\text{-}Pt(C_6F_5)_2(C{\equiv}CFc)_2]^{2-}$ (Figure S18), Model 1 (Figure S19), Model 2 (Figure S20), and **3** (Figure S21). Selected distances (Å) and angles (deg) for **1**−**6** (Tables S1−S4). DFT optimized coordinates of $[trans\text{-}Pt(C_6F_5)_2(C{\equiv}CFc)_2]^{2-}$ (Table S5) and complete reference 37. This material is available free of charge via the Internet at http://pubs.acs.org.